Optical coherence tomography in coronary atherosclerosis assessment and intervention

Abstract | Since optical coherence tomography (OCT) was first performed in humans two decades ago, this imaging modality has been widely adopted in research on coronary atherosclerosis and adopted clinically for the optimization of percutaneous coronary intervention. In the past 10 years, substantial advances have been made in the understanding of in vivo vascular biology using OCT. Identification by OCT of culprit plaque pathology could potentially lead to a major shift in the management of patients with acute coronary syndromes. Detection by OCT of healed coronary plaque has been important in our understanding of the mechanisms involved in plaque destabilization and healing with the rapid progression of atherosclerosis. Accurate detection by OCT of sequelae from percutaneous coronary interventions that might be missed by angiography could improve clinical outcomes. In addition, OCT has become an essential diagnostic modality for myocardial infarction with non-obstructive coronary arteries. Insight into neoatherosclerosis from OCT could improve our understanding of the mechanisms of very late stent thrombosis. The appropriate use of OCT depends on accurate interpretation and understanding of the clinical significance of OCT findings. In this Review, we summarize the state of the art in cardiac OCT and facilitate the uniform use of this modality in coronary atherosclerosis. Contributions have been made by clinicians and investigators worldwide with extensive experience in OCT, with the aim that this document will serve as a standard reference for future research and clinical application.

Axial resolution
The minimum distance between two objects that can be resolved along the axial dimension.

Near-infrared
Light with wavelengths extending from 0.78 µm to 2.50 µm.

Cross-sectional images
The traditional mode for optical coherence tomography (OCT) images that displays a cross-section of the vessel with a circular shape.

A full list of authors and their affiliations appears at the end of the paper.

https://doi.org/10.1038/s41569-022-00687-9

Optical coherence tomography (OCT) is an imaging technology used to evaluate the microstructure of coronary arteries. The axial resolution of OCT is approximately 10–15 µm (REF.[1]), which is higher than that of intravascular ultrasonography (IVUS), meaning that OCT can characterize the superficial structure of the vessel wall in greater detail[2,3]. A consensus document dedicated to the methodology of OCT research was published a decade ago[4], and a huge number of cardiac OCT studies have since been published. Consequently, substantial advances have been made in our understanding of in vivo vascular biology, and the benefits of OCT in the management of coronary atherosclerosis have been established. Although the role of intravascular imaging in the management of patients has been described in several articles, this Review is the first comprehensive summary of the role of OCT as both a research tool and a clinical tool.

The utility of OCT depends on the correct acquisition and interpretation of images, as well as on knowledge of the currently available evidence. In this Review, we summarize the state of the art in cardiac OCT and facilitate the uniform use of this modality in coronary atherosclerosis. The original draft of this Review — on optimal image acquisition, accurate image interpretation, the importance of OCT findings, the role of OCT in percutaneous coronary intervention (PCI) and the future development of this modality — was prepared at Massachusetts General Hospital (Boston, MA, USA). Contributions from OCT experts in other countries were incorporated, and the final document was circulated to and endorsed by >100 experts in OCT worldwide. We hope that this Review will be broadly used as a standard reference for future research and the clinical application of cardiac OCT. At present, two major intracoronary optical-based imaging systems are commercially available: OCT made by Abbott Vascular and optical frequency domain imaging (OFDI) made by Terumo. Given that image interpretation is identical between the two systems, the following descriptions of OCT also apply to OFDI.

Foundations of OCT imaging

Physical principles

OCT is a near-infrared, light-based imaging modality that generates high-resolution cross-sectional images of tissue microstructure[1]. The penetration depth depends on the tissue type and ranges from 0.1 mm to 2.0 mm, which

Key points

- The appropriate use of optical coherence tomography (OCT) depends on the accurate interpretation and understanding of the clinical importance of OCT findings.
- In vivo diagnosis of plaque erosion with OCT could lead to a major shift in the management of patients with acute coronary syndromes.
- Detection by OCT of healed coronary plaque is important for understanding the mechanism of plaque destabilization and healing with rapid progression of atherosclerosis.
- Accurate detection by OCT of findings after percutaneous coronary intervention that could be missed by angiography has the potential to improve clinical outcomes.
- OCT has become an essential diagnostic modality for patients with myocardial infarction and non-obstructive coronary arteries.
- Insights from OCT into neoatherosclerosis could improve our understanding of the mechanisms of very late stent thrombosis.

is less than that of IVUS (8.0–10.0 mm). The physical principles of OCT imaging are detailed in BOX 1, and OCT equipment is described in BOX 2.

Image acquisition

OCT should be used with caution in patients with a single remaining patent vessel, markedly impaired renal function or a known allergy to contrast media. In lesions with near-complete or total occlusion of the artery, antegrade blood flow should be restored by pre-dilatation using an under-sized balloon or aspiration thrombectomy before OCT examination, to allow the flushing media to clear blood adequately from the artery. If subintimal wiring is suspected in cases of chronic total occlusion, OCT should not be performed because injection of flushing media can force the progression of coronary dissections. OCT catheters are sometimes unable to pass through severely narrowed, calcified or tortuous lesions or are unable to follow the guidewire in arteries such as the left circumflex with a sharp angle from the left main coronary artery. The use of a guide extension catheter might help to deliver the catheter into the left circumflex without prolapse.

If not contraindicated, image acquisition should be conducted after the administration of intracoronary nitroglycerin to minimize catheter-induced vasospasm, with appropriate attention to anticoagulation. OCT imaging catheters require careful purging with viscous, undiluted contrast media to remove air or blood before the interrogation. The OCT imaging catheter is advanced into the distal coronary artery over a standard angioplasty guidewire (0.014 inches). Automated OCT pullback is performed either during manual contrast injection through the guiding catheter using a syringe or automatically using a power injector (typical flush rate 4.0–5.5 ml/s for the left coronary artery and 3.0–4.0 ml/s for the right coronary artery at 300–400 psi).

Coaxial positioning of the guiding catheter into the coronary ostium is important to obtain optimal blood clearance. A ≥6-Fr diameter guiding catheter is recommended, but OCT imaging catheters also fit 5 Fr guiding catheters or 6 Fr guide extensions. A guiding catheter without side holes might facilitate blood clearance. OCT acquisition can be performed through guide extension catheters, allowing improved target-vessel intubation, providing high-quality images for coronary ostial lesions and reducing the volume of contrast medium required.

Highly viscous contrast solutions provide superior results; therefore, iso-osmolar contrast media are used for flushing. In patients with impaired renal function, low-molecular-weight dextran, normal saline or diluted contrast media can be used as a substitute for iso-osmolar contrast media. Importantly, however, low-molecular-weight dextran can also cause renal toxicity and should therefore be used with caution.

Safety data

In a prospective registry of 1,142 OCT procedures and 2,476 IVUS procedures, catheter-related complications were rare and the rate did not differ significantly between the two modalities (0.6% versus 0.5%, respectively; $P = 0.60$)[5]. Complications were either self-limiting after retrieval of the imaging catheter or easily treatable in the catheterization laboratory. In this study, three cases of transient ST-segment elevation, two cases of bradycardia, one case of coronary artery spasm and one case of thrombus formation were observed, with no major adverse events, prolongation of hospital stay or permanent harm in patients who underwent OCT[5].

Total contrast volume injected during a pullback should be minimized. In a retrospective study with a total of 4,467 OCT or OFDI pullbacks performed for unselected indications, ventricular fibrillation occurred in 31 pullbacks (0.7%)[6]. On multivariate analysis, contrast volume of the individual pullback was the only independent factor for predicting ventricular fibrillation, suggesting prolonged ischaemia as the probable cause. Contrast injection should be terminated as soon as imaging of the target segment has been completed. Given that OCT imaging necessitates the use of an additional contrast medium compared with IVUS, understanding the risk of acute kidney injury is important. In the OPINION trial[7], the volume of contrast used in OCT-guided PCI was significantly greater than that used in IVUS-guided PCI (mean 164 ml versus 138 ml; $P < 0.001$). No cases of contrast-induced nephropathy, defined as an increase in serum creatinine level of 0.5 mg/dl or a relative increase of 25% over baseline value within 72 h, were recorded for either modality[7]. In the ILUMIEN III trial[8], a greater total contrast volume was also reported in OCT-guided PCI than in IVUS-guided PCI (median 222 ml versus 190 ml; $P = 0.004$). The DOCTORS study[9] showed that the incidence of acute kidney injury, defined as an absolute increase in serum creatinine of 0.5 mg/dl from baseline, was only 1.6% with either OCT-guided or angiography-guided PCI in patients with acute coronary syndromes (ACS). Of note, patients with chronic kidney disease (estimated glomerular filtration rate <30 ml/min/1.73 m^2 or serum creatinine level >1.5 mg/dl) were excluded from these studies. Therefore, although the available data indicate that the increased volume of contrast used in OCT is not clinically relevant in patients without chronic kidney disease, and the requirement for dialysis is extremely rare, preprocedural hydration should be considered before OCT-guided PCI as a precaution.

Penetration depth
The depth within a tissue or object at which an OCT image signal has been attenuated (via scattering or absorption) to a level indistinguishable from the background noise.

Box 1 | **Physical principles of OCT imaging**

Optical coherence tomography (OCT) light is in the near-infrared range (wavelength 0.78–2.50 μm), typically with a wavelength of approximately 1.3 μm, which is not visible to the human eye[1]. OCT measures the time delay of the light that is reflected or backscattered from tissue and collected by the catheter, using a technique known as interferometry[1]. Light from the OCT system is split so that half travels to the patient (sample arm) through a catheter and the other half travels a predetermined distance (reference arm). After being reflected from tissue and collected by the catheter, the difference between the sample arm and the reference arm is measured by a detector. When the distances that the sample and reference arm lights have travelled are roughly equivalent, a pattern of high and low intensities is detected, known as interference. This interference pattern is analysed by the OCT system to determine the amount of backscattering as a function of delay in time or depth within the tissue (A-line). A cross-sectional OCT image is obtained by recording A-lines as the beam is scanned across the sample by rotating the optics in the catheter. The axial range over which an OCT image can be obtained is termed the ranging depth; this parameter is typically 4–6 mm. Penetration depth is a term that defines how deeply within tissue that OCT image data that are higher than background noise can be obtained. As the light passes through tissue, it is attenuated by scattering and absorption. The predominant form of attenuation encountered by OCT systems is scattering. Highly attenuating tissue, such as lipid, has a low penetration depth; therefore, OCT does not visualize as deeply in lipid-containing plaques. Other tissues, such as collagen and calcium, have lower attenuation, and OCT can visualize deeper into these tissues. Therefore, the penetration depth in arteries depends on tissue type and usually ranges from 0.1 mm to 2.0 mm using typical OCT near-infrared light. OCT cannot image through blood because blood scatters the OCT light before it reaches the artery wall. As a result, in vivo acquisition of intracoronary OCT images requires the displacement of blood from the field of view using a flushing medium. OCT images are acquired using a spiral scan pattern, analogous to intravascular ultrasonography. The OCT optical components in the catheter are rapidly rotated to acquire cross-sectional images, while simultaneously pulling back to volumetrically image a vessel segment. Rotation and pullback interrogation are conducted via a motorized proximal unit.

Image display

Three modes are available for displaying OCT images — the traditional cross-sectional image (orthogonal to the vessel), the longitudinal (L-mode) view and 3D visualization (BOX 3). Contemporary OCT systems provide co-registration with angiography to allow cross-sectional OCT images to be matched with their position on angiograms, which facilitates plaque assessment and optimization of PCI.

Artefacts

The recognition of artefacts is crucial for the correct interpretation of images. Representative images of OCT artefacts are shown in FIG. 1.

Guidewire. The guidewire blocks the OCT light beam and causes a shadow, so that tissue and stents behind the wire cannot be seen (FIG. 1a). Removal of the guidewire before OCT image acquisition can be considered when visualization of the area blocked by the guidewire artefact is crucial. However, caution should be exercised with guidewire removal to avoid trapping the OCT catheter or damaging the vessel wall, particularly in distal segments or heavily calcified or tortuous vessels.

Gas bubbles. Inside fluid-filled catheters, gas bubbles can be recognized as distinct focal bright regions and a diminished signal in the part of the OCT image in the path of the affected region of the catheter (FIG. 1b). Gas bubbles can form inside the OCT catheter if the operator does not adequately flush the catheter before introduction into the guiding catheter. Gas bubbles can also appear in the lumen of the vessel, injected through the guiding catheter, causing the appearance of a bright outline of the bubble and a shadow on the OCT image behind the bubble.

Suboptimal vessel flushing. Amorphous bright features can be present in the OCT image when blood is inadequately cleared from the field of view because erythrocytes scatter light (FIG. 1c). When mixed with optically transparent flushing media, blood can form many different patterns within the artery lumen. Blood can be confused with red thrombus or vessel wall dissections. Blood attenuates the OCT signal and can therefore prohibit adequate tissue characterization. Automatic detection of lumen, strut apposition and calcification is especially susceptible to blood artefact.

Thrombi. Red blood cells scatter light; therefore, when a red thrombus is positioned between the catheter and the arterial wall, a shadow will appear beyond the thrombus, diminishing the intensity of the signal from the arterial wall (FIG. 1d). Shadow effects are greatest for thrombi positioned closest to the catheter.

Macrophages. Macrophage accumulations can create shadows in the image, potentially causing a plaque to appear to be a thin-cap fibroatheroma (TCFA) (FIG. 1e).

Ghost lines. Appearing as circular features around the OCT catheter (FIG. 1f), ghost lines are caused by light reflections from interfaces within the catheter or optical connections between the OCT instrument and catheter. These artefacts should be identified and not interpreted as the OCT catheter sheath. If ghost lines are misinterpreted and used for calibration, measurements will be artefactually reduced.

Non-uniform rotational distortion. Variations in the rotation rate of the catheter torque cable and distal optics cause non-uniform rotational distortion, which appears as a blurring or smearing in the lateral (or rotational) direction (FIG. 1g). Non-uniform rotational distortion is normally caused by mechanical rotational resistance in the catheter owing to either a tortuous or narrow vessel, a tight haemostatic valve, a crimped catheter sheath or a defective catheter.

Fold-over artefacts. When the vessel diameter is larger than the ranging depth, a portion of the vessel can appear to fold over in the OCT image (FIG. 1h). Portions of the image that contain fold-over artefacts should not be interpreted.

Tangential signal dropout. When the catheter is located very near to the vessel wall, the optical beam can be directed almost parallel to the tissue surface. In these situations, the light beam is attenuated as it passes along the surface of the artery wall, which can appear signal-poor below the luminal surface (FIG. 1i). This artefact is often confused with the appearance of

L-mode
The longitudinal mode represents an OCT image along the longitudinal dimension at a particular rotational angle.

Co-registration
The process of registering two or more images so that they can be viewed and analysed together.

Backscattered light
The reflection of light back in the direction from which it came; usually a diffuse reflection due to scattering as opposed to specular reflection as from a mirror.

Leading edge
The first edge in an object that is encountered along a vector that is pointing away from the catheter; by contrast, the trailing edge is the last edge that is encountered.

Z-offset
Slight variations in optical path length within the catheter, which can be adjusted using the catheter diameter within an image as a reference.

Refractive index
A property of a material that governs the speed of light through that material.

Centroid
The arithmetic mean position of all the points in the figure; also known as the centre of mass.

Adluminal
Near or towards the lumen.

Pullback rate
The speed at which an OCT catheter is pulled back during imaging.

TCFA, intimal disruption or superficial accumulation of macrophages.

Seam artefacts. When the catheter moves with respect to the vessel during single cross-sectional image acquisition, an axial discontinuity termed a seam artefact (FIG. 1j) can appear at the location of the transition between the first and the last axial scans.

Beam divergence. When the imaging catheter is very near to or touching the arterial wall, the solid angle between the backscattered light and pupil of the imaging catheter is increased so that the OCT signal level can be relatively brighter than the light backscattered from tissue regions far from the catheter (FIG. 1k). Alternatively, when the backscattered light originates from a position further than the beam focus, a larger spot size and smaller solid angle contribute to the reduced OCT signal intensity.

Blooming. An increase in strut reflection thickness in the axial direction of OCT images (FIG. 1l) causes the small, bright-line segment that represents the leading edge of a stent strut to appear thicker than normal, making it difficult to locate the true leading edge of the strut.

Saturation. When a high reflector is encountered by OCT light, it can be backscattered at too high an intensity to be accurately detected, thereby causing saturation artefact (FIG. 1m). Structures that exhibit high backscattering commonly include the guidewire, the tissue surface and metallic stent struts. Saturation artefacts appear as linear streaks of high and low intensities within the image along the axial direction.

Merry-go-round artefacts. Merry-go-round artefacts are small, bright-line segments representing stent struts that appear elongated in the lateral (rotational) direction (FIG. 1n). Optical scattering in the lumen (primarily due to inadequate blood flushing) between the catheter and arterial wall can cause the light backscattered from stent struts to appear to originate from a wider arc length than the true strut length.

Sunflower artefacts. When the OCT catheter is located in an eccentric position in the vessel, metallic stent struts can appear to curve towards the OCT catheter (like flowers growing towards the sun) (FIG. 1o). This artefact can cause a well-apposed stent to appear malapposed in the vessel because incident OCT light reflects from only a small region of the edge of the strut (not the entire strut) back to the catheter.

Morphologies and measurements

Basic measurements

The reproducibility of OCT measurements is reportedly high[10–12]. Meaningful measurements require good-quality images that contain no or minimal artefacts. Although OCT systems provide automatic lumen detection, manual correction is required, especially when the image quality is suboptimal. To make accurate measurements, the image should be correctly calibrated for the z-offset (slight variations in optical path length within the catheter, which can be adjusted using the catheter diameter within an image as a reference) and refractive index of the flushing medium. OCT systems also offer automated calibration but manual correction is sometimes required. Measurements can be inaccurate when the OCT catheter is not coaxial with the vessel centreline. However, perfect coaxial alignment is difficult to achieve in the real world. Proximal or distal reference is defined as the site with the largest lumen proximal or distal to a stenosis but within the same segment (usually within 10 mm of the stenosis, with no major intervening branches)[4], which might not be the site with the least plaque.

The definitions of basic measurements are as follows:

- Arc: measured using the lumen centroid as the vertex.
- Depth: the distance between the luminal border and the adluminal surface of the plaque feature.
- Thickness: the thickest distance between the inner and outer border of the plaque component (valid only if the deep boundary can be identified).
- Area: the cross-sectional area of the plaque component (valid only if the deep boundary can be identified).
- Volume: the sum of areas of each cross-section multiplied by the slice thickness over the segment of interest (Simpson rule).
- Cap thickness: the thickness of a cap present over calcium or lipid. Minimum fibrous cap thickness is conventionally measured three times at the thinnest point in magnified views, and the average value is calculated[13]. The location of minimum fibrous cap thickness is searched throughout the plaque by visual inspection. This approach involves the risk of selection bias with intraobserver and interobserver variability. For increased objectivity, semi-automated assessment of cap thickness[14] or 3D measurement of the surface area of the thin fibrous cap[15] have been proposed.
- Lesion length: the distance between the proximal and distal reference. Length measurements can be obtained in OCT data sets that are acquired using automated pullback. The slice thickness (image spacing) in millimetres is the pullback rate (millimetres

Box 2 | **OCT equipment**

Two types of optical coherence tomography (OCT) systems are available: initial time-domain OCT and newer, higher speed frequency-domain OCT systems (FD-OCT; also known as swept-source OCT or optical frequency domain imaging (OFDI)) (see the table). Time-domain OCT was first reported in 1997 (REF.[149]) and FD-OCT in 2003 (REF.[150]). Only FD-OCT is currently being used for coronary evaluation. Automated pullback speeds of current systems are 18 or 36 mm/s for OCT and 10, 20, 30 or 40 mm/s for OFDI. Interrogation lengths are 54 or 75 mm for OCT and up to 150 mm for OFDI.

Parameter	OCT	OFDI
Basic technology	Frequency domain	Frequency domain
Size of catheter (Fr)	2.7	2.6
Pullback speed (mm/s)	18 or 36	10, 20, 30 or 40
Pullback length (mm)	54 or 75	Up to 150
Centre of wavelength (μm)	1.3	1.3
Axial resolution (μm)	10–15	<20

Box 3 | **OCT image display techniques**

Cross-sectional display

The cross-sectional display is the traditional mode for optical coherence tomography (OCT) images and displays a cross-section of the vessel with a circular shape.

L-mode display

The L-mode display is a longitudinal section or longitudinal reconstruction of an OCT pullback data set at a particular rotational angle (see the figure, panel **a**). The plane through which the longitudinal section is taken should intersect the centre of the catheter. Lesion length measurements can be made using L-mode images because the frame rate and pull-back speeds are known. The severity of stenosis can be shown on an L-mode display. However, OCT catheters are not always coaxial to the centre of mass of the lumen and eccentric lesions are common; therefore, L-mode should always be evaluated with reference to the cross-sectional lesions because apparent stenoses in the L-mode view can be underestimated or overestimated. Care should be taken when interpreting L-mode images because motion artefacts can cause the appearance of repeated structures, the disappearance of structures or oscillation of the artery wall microstructure. L-mode image quality also depends on frame-to-frame spacing, which affects the resolution along the longitudinal dimension. Importantly, the L-mode view can provide a misleading impression of the minimum lumen area location, depending on catheter localization.

3D visualization

3D visualization, including cutaway or flythrough views of volume renderings (see the figure, panels **b**,**c**), has been used to display OCT data sets. These representations include multiple frames of a pullback, rather than showing only one cross-sectional image at a time. The implementation of strut-detection algorithms enables stent structures to be visualized in the coronary artery in relation to the arterial wall. These methods of visualization are advantageous because they can efficiently provide an overview of the artery wall anatomy and elucidate the anatomy of bifurcations. The 3D view could be helpful in percutaneous coronary intervention of bifurcation lesions and, in particular, in the assessment of recrossing a guidewire to the side branch. Of note, plaque morphology should be assessed using cross-sectional OCT images rather than with 3D visualization.

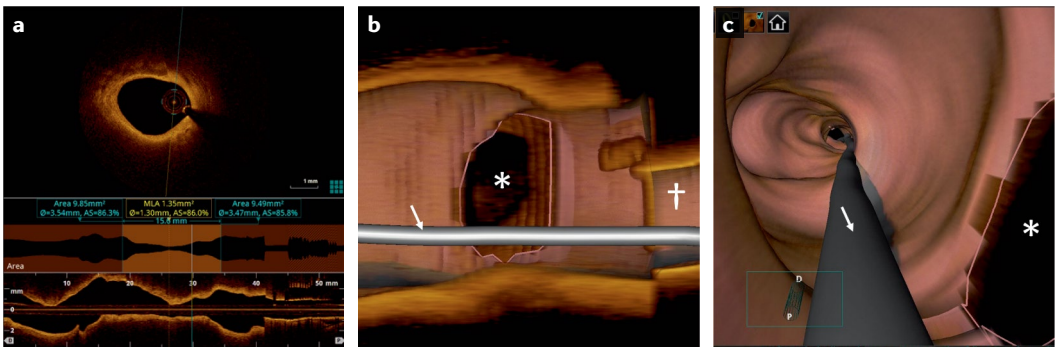

a | L-mode display. **b** | 3D cutaway view. **c** | 3D flythrough view. The asterisks indicate a side branch. The arrows indicate the guidewire. The dagger indicates a guiding catheter. Φ, diameter; AS, area stenosis; MLA, minimum lumen area.

per second) divided by the frame rate (per second). When the vessel is curved, length measurements for an object located far from the OCT catheter become inaccurate.

Vessel and plaque morphology

Given that OCT acquires multiple sequential images during pullback, confirming a finding in more than one frame helps to improve diagnostic confidence. The following image interpretations are widely accepted.

Normal vessel wall. The media of a normal vessel appears as a band of lower signal intensity relative to that of the intima and adventitia, providing a three-layered appearance (bright–dark–bright) (FIG. 2a). The internal elastic membrane (IEM) is defined as the border between the intima and media, and the external elastic membrane (EEM) is defined as the border between the media and the adventitia. These membranes can be visualized as highly backscattering, thin structures. Intimal thickening occurs during the early phase of coronary atherosclerosis[16] and is represented as a signal-rich, homogeneous, thick intimal band in OCT images (FIG. 2b). The definition of intimal thickening is limited by the lack of an established cut-off value.

Atherosclerotic plaque. Atherosclerotic plaques are identified as a mass lesion (focal thickening) or by the loss of the layered structure of the vessel wall.

Fibrous plaque. Fibrous plaques are homogeneous, signal-rich (high-backscattering) regions (FIG. 2c). Sometimes, the limited penetration depth of OCT precludes accurate detection of signal-poor regions located deep within the vessel wall, thereby limiting the assessment of lipid or calcium behind fibrous tissue.

Calcified plaque. Calcified plaques are signal-poor regions with sharply delineated borders and limited shadowing (FIG. 2d). Light penetrates calcium; therefore, unlike IVUS, OCT can be used to quantify both the arc and thickness[17] of calcification, providing it is not positioned at depth in direct contact with the adventitia and is not thicker than the penetration depth

Frame rate
The number of images captured per second.

Attenuation
Loss of light due to scattering and/or absorption by flushing media, blood or tissue that results in a weaker OCT signal.

of light[18]. Calcification thickness can be measured only when both the leading and trailing edges are visible. Calcium deposit length is measured on the longitudinal view. Calcium index is calculated as the product of calcium arc and calcium length[19]. In 2018, a novel calcium scoring system was proposed for the prediction of stent underexpansion[20]. Two points are given for a maximum angle >180°, one point for maximum calcium thickness >0.5 mm and one point for calcium deposit length >5 mm. Lesions with a score of four points had poor stent expansion[20]. The European Association of PCI (EAPCI) expert consensus document on the clinical use of intracoronary imaging states that a calcium arc >180° and a calcium deposit thickness >0.5 mm are risk factors for stent underexpansion[21]. These measurements can have a bearing on how best to prepare a calcified lesion before stent implantation.

Lipid plaque. Lipid plaques are signal-poor regions with diffuse borders (lipid pool) and overlying signal-rich bands (fibrous caps), accompanied by high signal attenuation (FIG. 2e). Histopathological validation studies show a good correlation between signal-poor OCT regions with diffuse borders and lipid pools on histology,

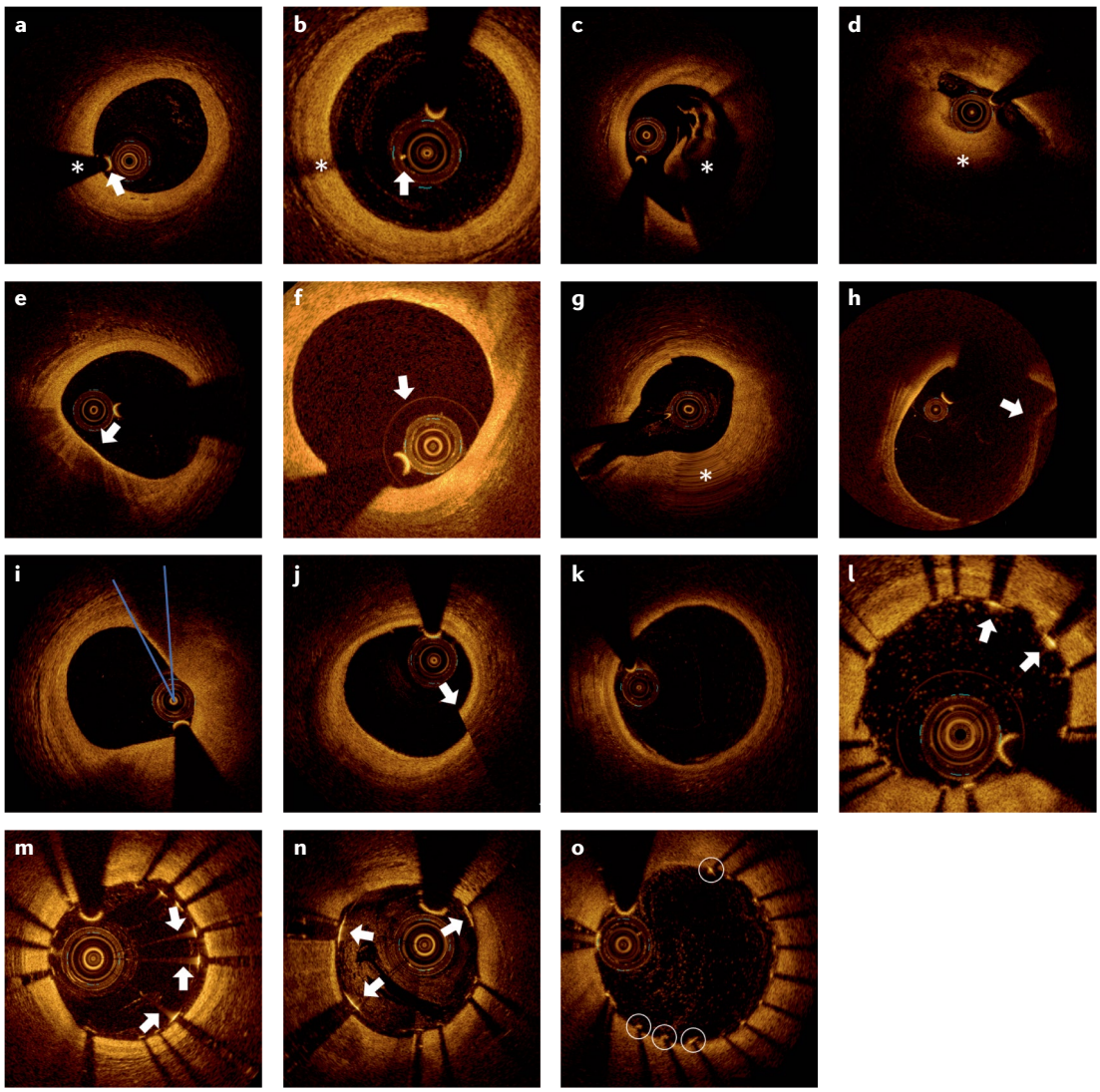

Fig. 1 | **Artefacts on optical coherence tomography. a** | The guidewire (arrow) causes a shadow (asterisk). **b** | Gas bubbles in the catheter (arrow) cause a shadow (asterisk). **c** | Suboptimal vessel flushing leads to residual blood in the lumen (asterisk), hampering the assessment of the vessel. **d** | Thrombus (asterisk) casts a shadow, diminishing the intensity of the signal from the arterial wall. **e** | Macrophages mimicking thin-cap fibroatheroma (arrow). **f** | Ghost lines (arrow). **g** | Non-uniform rotational distortion (asterisk). **h** | Fold-over artefact (arrow). **i** | Tangential signal dropout; blue lines indicate the direction of light beams tangential to the tissue that appears to have an artefactual light dropout. **j** | Seam artefact (arrow). **k** | Beam divergence; the tissue near the catheter is very bright, whereas the rest of the area is dimmer; the brighter region (9 o'clock) has a higher resolution than the dimmer area (3 o'clock). **l** | Blooming; stent struts (arrows) appear thicker than they actually are. **m** | Saturation; a high signal intensity artefact (arrows) extends along the axial dimension. **n** | Merry-go-round artefact; artefactual stretching in the lateral (rotational) direction of stent struts (arrows) resulting from scatters in the lumen such as residual blood, clots and neointima. **o** | Sunflower artefact can cause a well-apposed stent to appear malapposed in a vessel (white circles).

Speckle
The grainy pattern that appears in OCT images because of the interference of waves with random phase.

corresponding to either a necrotic core or a region within pathological intimal thickening that contains extracellular lipid, proteoglycans or both[3,22]. Owing to the limited penetration depth of OCT in lipid-containing tissues, OCT cannot be used to measure the thickness, area or volume of lipids. Instead, the circumferential arc is used to semi-quantify lipids. Lipid-rich plaque is defined as plaque that has a lipid arc of >90° (REF.[23]). Lipid deposit length is measured on the longitudinal view. Lipid index is calculated as the product of the mean lipid arc and the lipid deposit length[24].

Thin-cap fibroatheroma. TCFA is defined as a lipid plaque in which the minimum thickness of the fibrous cap is less than a predetermined threshold, and lipid occupies >90° in circumference (FIG. 2f). The most frequently adopted cut-off value for minimal cap thickness is 65 µm, derived from histology studies[25]. However, caution should be taken when this cut-off value is applied directly to OCT because tissue shrinkage can occur during histopathological tissue processing and only samples from patients who died were assessed. Therefore, the true minimum fibrous cap thickness that can predispose plaques to rupture could be >65 µm, and a cut-off thickness of 80 µm is sometimes used[26]. Semi-automated assessment of cap thickness[14] and 3D measurement of the surface area of the fibrous cap[15] have been reported. Tangential signal dropout (FIG. 1i) and macrophages (FIG. 1e) can falsely create the appearance of a TCFA.

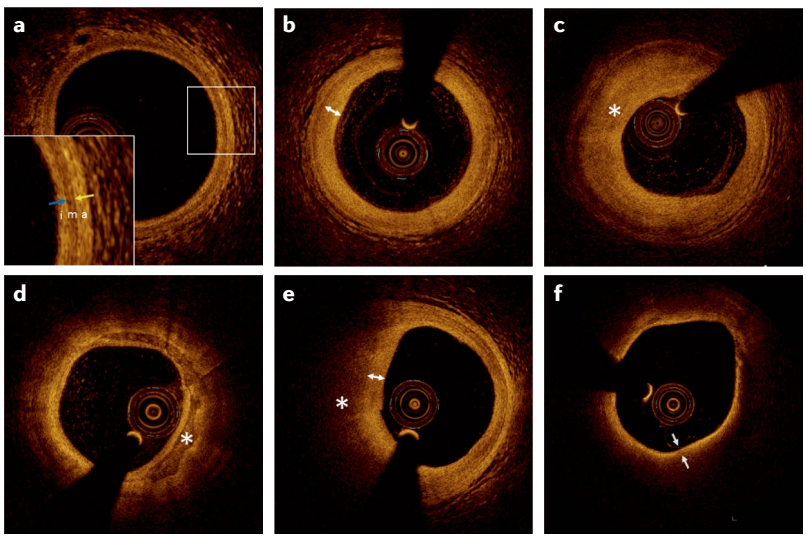

Fig. 2 | **Optical coherence tomography images of normal vessel and atherosclerotic plaques. a** | Normal vessel wall is characterized by a three-layered architecture comprising a high-backscattering, thin intima (i), a low-backscattering media (m), a high-backscattering adventitia (a), an internal elastic membrane as the border between the intima and media (blue arrow), and an external elastic membrane as the border between the media and the adventitia (yellow arrow). **b** | Intimal thickening occurs during the early phase of atherosclerosis in the coronary artery, which is represented as a signal-rich, thick intimal band (double-headed arrow). **c** | Fibrous plaque appears as homogeneous, signal-rich (highly backscattering) regions (asterisk). **d** | Calcified plaque appears as signal-poor regions with sharply delineated borders and limited shadowing (asterisk). **e** | Lipid-rich plaque appears as signal-poor regions (asterisk) with diffuse borders and overlying signal-rich bands (double-headed arrow). **f** | Thin-cap fibroatheroma is a lipid-rich plaque in which the minimum thickness of the fibrous cap (arrows) is less than a predetermined threshold, and the lipid deposit occupies >90° in circumference.

Macrophages. Macrophages are inflammatory cells that can be located in the fibrous tissue covering a lipid plaque and occasionally in fibrous plaque. Macrophages appear in OCT images as signal-rich, distinct or confluent punctate regions that exceed the intensity of background speckle noise[27] (FIG. 3a). Owing to their high backscattering and attenuation characteristics, macrophages cast a dark shadow behind their aggregates. Macrophages frequently cluster together, forming a band of highly reflective tissue, which can cause a plaque to appear to be a TCFA (FIG. 1e). The strong attenuating properties of macrophage aggregates cause the casting of a laterally sharp shadow and a rapid change in appearance from frame to frame. These typical characteristics help to differentiate a band of macrophages overlying a fibroatheroma from a true TCFA. A detailed classification of macrophages into lines or dots has been reported[28]. Quantification of macrophages has been attempted using a parameter termed the normalized standard deviation[27]. Semi-quantification (grade 0–4) has also been reported[29]. Importantly, rigorous histological validation of macrophages on OCT imaging has not yet been reported.

Microvessels. With increasing plaque size, nurturing vessels known as microvessels (or microchannels) gradually develop. Microvessels promote the influx of lipids and inflammatory or red blood cells into coronary plaques[30]. Microvessels in the intima can appear in OCT images as signal-poor voids that are sharply delineated and can usually be followed in multiple contiguous frames[31] (FIG. 3b). A cut-off diameter of 50–300 µm and a requirement for the extension to be present in at least three consecutive frames are sometimes adopted to define microvessels[31]. As microvessels communicate with the periadventitial vasculature and eventually with the lumen of the coronary artery, their blood content is flushed during an OCT pullback. To discriminate between larger microvessels and small side branches, an inspection of adjacent frames is helpful. The accuracy of microvessel detection decreases in lipid-rich plaques, in which the penetration of OCT light is hampered. Whether microvessels communicate with the luminal surface or emanate from the vasa vasorum has not been established. Detection and quantification of adventitial vasa vasorum have been attempted[32,33], but further studies are required to explore this issue.

Cholesterol crystals. Cholesterol expands in volume when crystallizing from a liquid to a solid state and can cause plaque volume expansion[34]. Both ex vivo human studies and animal studies suggest that sharp-tipped cholesterol crystals can perforate the fibrous cap[35]. Cholesterol crystals appear in OCT images as thin, linear regions of high intensity, usually in proximity to a lipid-rich plaque (FIG. 3c). In histology studies, the sensitivity of OCT for detecting cholesterol crystals has been reported to be 68%[36] and 26%[37], even after a modification to the definition of cholesterol crystals in the latter study[37]. Of note, some cholesterol crystals identified in histology are not visualized by OCT, particularly when cholesterol crystals are aligned tangentially to the OCT light beam.

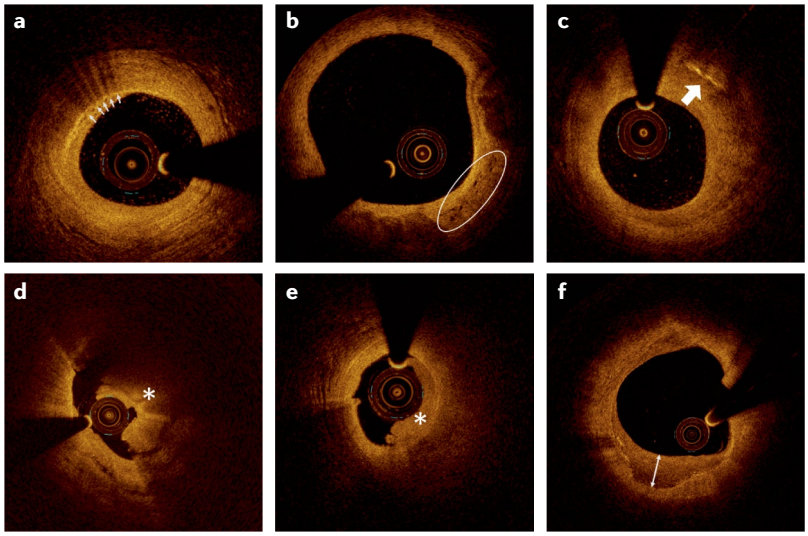

Fig. 3 | **Qualitative findings from optical coherence tomography. a** | Macrophages are seen as signal-rich, distinct or confluent punctate regions that exceed the intensity of background speckle noise and cast a dark shadow (arrows). **b** | Microvessels within the intima can appear as signal-poor voids that are sharply delineated and can usually be followed in multiple contiguous frames (white oval). **c** | Cholesterol crystals appear as thin, linear regions of high intensity (arrow), usually in proximity to a lipid-rich plaque. **d** | A thrombus is seen as an irregular mass protruding into the lumen; red thrombus is seen as a high-backscattering protrusion with signal-free shadowing, which diminishes the signal intensity originating from the arterial wall (asterisk). **e** | White thrombus is seen as a signal-rich, homogeneous backscattering projection, which does not obscure the vessel (asterisk). **f** | Layered plaque; the double-headed arrow indicates a layer of different optical densities.

Thrombi. Destabilization of plaque leading to subsequent thrombotic occlusion of the coronary artery accounts for the majority of ACS. On OCT images, a thrombus appears as a protruding mass attached to the luminal surface or floating within the lumen. OCT can discriminate between two types of thrombi: red (erythrocyte-rich) thrombi (FIG. 3d), which are highly backscattering and have high attenuation (resembling blood), and white (platelet-rich) thrombi (FIG. 3e), which are less backscattering, homogeneous and have lower attenuation. Given that red blood cells reflect light, red thrombi typically shadow or obscure underlying structures, whereas platelet thrombi do not. Spontaneous recanalized coronary thrombi can appear as signal-rich, high-backscattering septa dividing the lumen into multiple small cavities with smooth inner borders, known as a 'honeycomb' appearance[38,39]. However, this finding requires histological validation. The thrombus score is calculated by summing the number of involved quadrants (0, 1, 2, 3 or 4) in each cross-sectional image through the longitudinal length of the thrombus[40]. The thrombus area is measured by tracing outlines of the thrombus on cross-sectional images. The thrombus volume is calculated by mean thrombus area multiplied by thrombus length[41].

Layered plaque. Pathology studies have shown that atherosclerotic plaques can destabilize without clinical consequences[42,43]. Whether ACS develops after disruption of a plaque depends on the severity of stenosis and the balance between systemic or local thrombogenicity and endogenous antithrombotic and thrombolytic mechanisms. Over the course of days or weeks, a silently developed thrombus becomes organized, with connective tissue deposition of, predominantly, proteoglycans and type III collagen[44,45]. During the healing process, type III collagen is gradually replaced by type I collagen, which appears as a band of high-backscattering signal on OCT images[44,45]. In a histological validation study, excellent agreement was reported between healed plaques on pathology and layered plaques on OCT images[46]. Layered plaque is defined as plaque with one or more layers of different optical densities and a clear demarcation from underlying components[44] (FIG. 3f). Serial OCT assessments in large and well-characterized study populations are required to better understand the process of plaque destabilization and healing.

Intraplaque haemorrhage. OCT has not been validated for the diagnosis of intraplaque haemorrhage. Only two case reports have been published so far, in which OCT images showed a clearly bordered, crescent-shaped, low-signal region[47,48]. Histological validation studies are required for this finding.

Aneurysms. Defining aneurysmal or ectatic coronary segments angiographically can be challenging, especially because most recognized definitions require comparison against a 'normal' vessel segment. Therefore, when uncertainty exists, intravascular imaging can be used to clarify the underlying vessel morphology. In aneurysms exceeding a diameter of ~5 mm, IVUS is the preferred imaging modality owing to its depth of penetration, facilitating the evaluation of large vessel dimensions. A true aneurysm is a lesion that includes three layers of the vessel wall, with an EEM and lumen area >50% larger than the proximal reference segment. Pseudoaneurysm is identified by disruption of the EEM, usually observed after an intervention. OCT can also be used for the evaluation of coronary aneurysms, although constraints relating to the limited ranging depth of OCT should be considered because the catheter tends to have an eccentric position within the lumen.

Transplantation vasculopathy. Cardiac allograft vasculopathy (CAV) is a leading cause of long-term death after heart transplantation. Intravascular imaging can be used to understand the pathophysiology of CAV and help to manage patients[49]. Early CAV takes the form of diffuse intimal thickening, whereas atherosclerotic changes develop later. OCT, with its capacity to detect early intimal changes, is the modality of choice to diagnose and monitor the progression of CAV. Cassar et al. reported the development of atherosclerosis with vulnerable plaque and complex coronary lesions in cardiac allografts[50]. When compared with native atherosclerosis, CAV was found to be associated with previous high-grade cellular rejection, and with homogeneous coronary lesions that had increased intimal thickening and macrophage infiltration[51,52]. The presence of many microvessels has also been observed[52,53]. Homogeneous, signal-rich tissue in a layered pattern is a frequent finding in CAV and has been reported to be a predictor of CAV progression[54,55].

Lumen measurements

When the lumen has been traced, the following lumen measurements can be made:

- Lumen area: the area bounded by the luminal border.
- Minimum lumen diameter: the shortest diameter through the centre of mass of the lumen.
- Maximum lumen diameter: the longest diameter through the centre of mass of the lumen.
- Lumen eccentricity: the (maximum lumen diameter minus the minimum lumen diameter) divided by the maximum lumen diameter.
- Minimum lumen area: the smallest lumen area along the length of the target lesion.
- Percent area stenosis: the (reference lumen area minus the minimum lumen area) divided by the reference lumen area, multiplied by 100. The reference segment used should be specified (proximal, distal, largest or average).

IEM measurements

For plaques in which the IEM can be identified, area and diameter can be measured for the IEM. In the presence of a large plaque burden or lipid deposit, OCT cannot visualize the entire circumference of the IEM. Consequently, the following IEM measurements can be made only for those plaques in which the IEM can be identified for ≥180°:

- Plaque area: the cross-sectional area of the IEM minus the cross-sectional area of the lumen.
- Maximum plaque thickness: the longest distance from the intimal leading edge to the IEM along any line passing through the centre of mass of the lumen.
- Minimum plaque thickness: the shortest distance from the intimal leading edge to the IEM along any line passing through the centre of mass of the lumen.
- Plaque eccentricity: the (maximum plaque thickness minus the minimum plaque thickness) divided by the maximum plaque thickness.
- Plaque burden: plaque area divided by the cross-sectional area of the IEM.
- Remodelling: the cross-sectional area of the lesion IEM divided by the cross-sectional area of the reference IEM.

These measurements can also be applied to the EEM. An attenuation compensation technique, a post-processing methodology to enhance the EEM, has been reported[56,57].

OCT for specific investigations

Mechanisms of ACS

OCT can accurately assess vessel and lumen geometry and identify the hallmark of a culprit lesion, including plaque disruption and thrombus. An improved understanding of the mechanisms of ACS has the potential to change the management of a subset of patients with ACS. FIGURE 4 shows a flow chart of a possible treatment algorithm for patients with ACS based on the assessment of microstructures by OCT. Importantly, however, many important steps lack evidence from randomized controlled trials and are potential avenues for future research. Conservative management without stenting for patients with plaque erosion is suggested only in proof-of-concept studies[24–27].

Plaque rupture. Plaque rupture can be identified by a disrupted fibrous cap, with communication between the lumen and the inner core of the plaque[58] (FIG. 5a). When injected with optically transparent contrast media, the disruption can appear as a hollow cavity. Thrombi

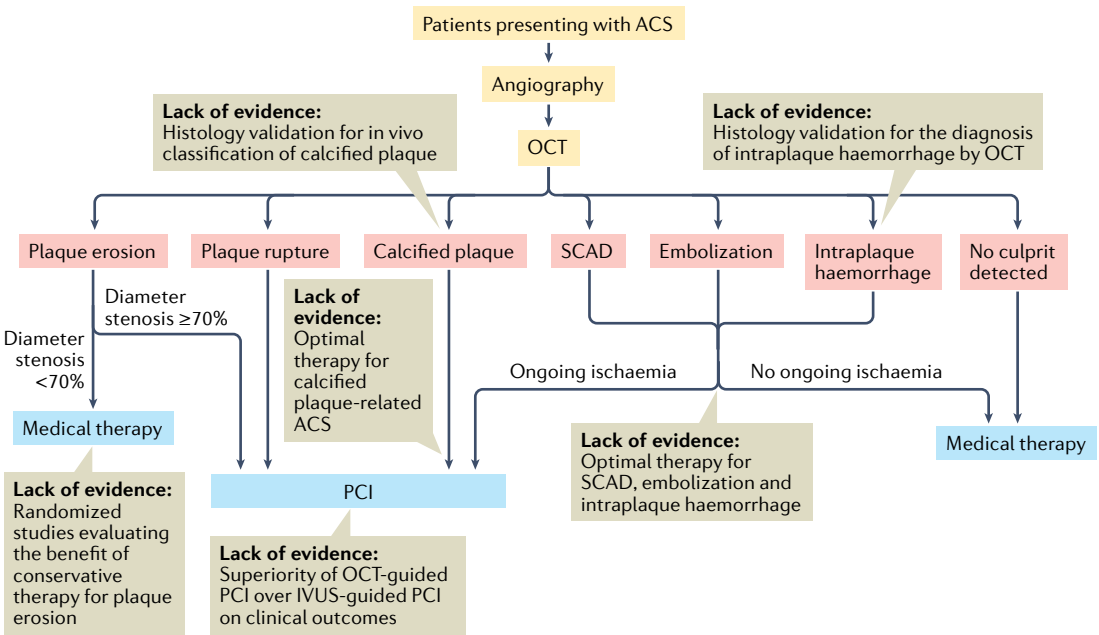

Fig. 4 | **Possible treatment algorithm for patients with ACS based on the assessment of microstructures by OCT.** Note that some important steps lack evidence from randomized controlled trials. ACS, acute coronary syndromes; IVUS, intravascular ultrasonography; OCT, optical coherence tomography; PCI, percutaneous coronary intervention; SCAD, spontaneous coronary artery dissection.

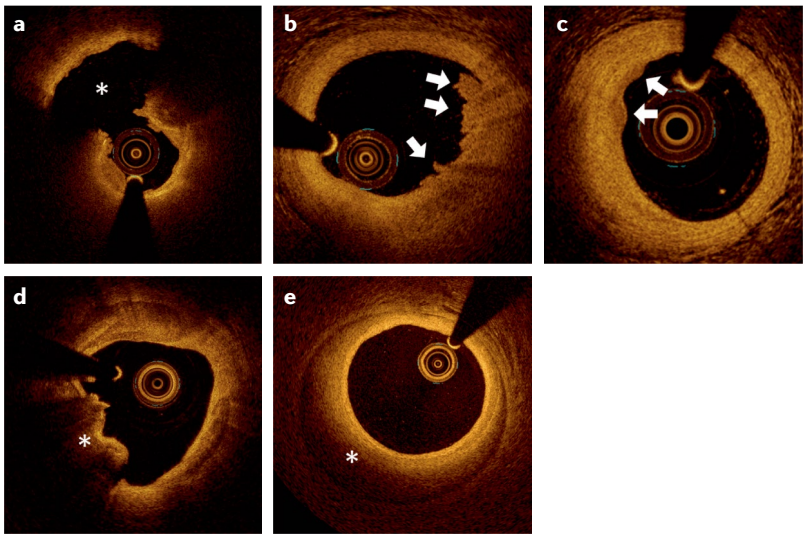

Fig. 5 | **Optical coherence tomography images of culprit lesions in patients with acute coronary syndromes. a** | Plaque rupture is characterized by the presence of fibrous cap discontinuity with a cavity formation (asterisk) within the plaque. **b** | Definite plaque erosion is characterized by the presence of attached thrombus (arrows) overlying an intact and visualized plaque. **c** | Probable plaque erosion is characterized by luminal surface irregularity (arrows) at the culprit lesion in the absence of thrombus. **d** | An eruptive calcified nodule appears as single or multiple regions of calcium that protrude into the lumen, with fibrous cap disruption frequently forming sharp, protruding edges, and the presence of substantive calcium proximal and/or distal to the lesion (asterisk). **e** | Spontaneous coronary artery dissection is seen as a separation of the intima and media from the adventitia (intramural haematoma) (asterisk), with or without communication with the vessel lumen (intimal tear).

are often found overlying the ruptured cap; however, thrombi can be absent at the site of an old plaque rupture or with acute rupture treated with antithrombotic or thrombolytic therapies. The presence of a large, luminal red thrombus obscures the underlying component, rendering a reliable diagnosis of plaque rupture difficult. Assessing contiguous frames, rather than a single frame, helps to differentiate between plaque rupture and other components such as side branches and artefacts.

Plaque erosion. Plaque erosion is the mechanism underlying 25–60% of ACS[59–61]. The pathology definition of plaque erosion is endothelial denudation with thrombosis, without evidence of plaque rupture[58]. The detection of an endothelial monolayer (1–5 μm) is below the resolution of the current OCT systems; therefore, plaque erosion remains a diagnosis of exclusion in vivo. Moreover, no diagnostic method is currently available to identify plaque that is likely to develop superficial endothelial denudation and occlusive thrombus formation.

In the algorithm developed for the classification of culprit plaques in patients with ACS[62], definite erosion was defined by the presence of attached thrombus overlying an intact and visualized plaque (FIG. 5b). Probable erosion was defined by luminal surface irregularity at the culprit lesion in the absence of thrombus (FIG. 5c) or attenuation of underlying plaque by thrombus without superficial lipid deposition or calcification immediately proximal or distal to the site of thrombus. An algorithm for the diagnosis of plaque erosion is presented in Supplementary Figure 1. As these criteria lack the precision of the pathology definition of erosion, some studies refer to this entity as an intact fibrous cap[63]. Plaque erosion is predominantly accompanied by white rather than red thrombi. When a large red thrombus is present, which attenuates the OCT light, the diagnosis of plaque erosion becomes less definite because plaque rupture cannot be excluded. Identification of plaque erosion can facilitate the tailoring of treatment. Proof-of-concept studies have demonstrated that plaque erosion associated with a residual diameter stenosis <70% can be treated with antithrombotic therapy without stenting[64–67]. Large randomized controlled studies are needed to explore this concept further.

Eruptive calcified nodule. An eruptive calcified nodule is characterized by an underlying heavily calcified plaque with a distinct nodular mass of calcium that protrudes into the lumen and causes dysfunction or loss of the overlying endothelial cells[68]. Eruptive calcified nodules appear in OCT images as single or multiple regions of calcium that protrude into the lumen with fibrous cap disruption, frequently forming sharp, protruding edges, and the presence of substantive calcium proximal or distal to the lesion[18] (FIG. 5d). The attenuation of OCT light from protruding calcium conceals deeper structures, rendering differentiation from red thrombus difficult. Eruptive calcified nodules are typically found in elderly individuals or patients undergoing kidney dialysis, with heavily calcified vessels at hinge points. Eruptive calcified nodules are associated with an increased rate of target-vessel failure after PCI, highlighting the complex nature of this lesion[69]. A system of in vivo classification for calcific plaque-related ACS has been proposed[70], which includes eruptive calcified nodules, superficial calcific sheets (Supplementary Figure 2a) and calcified protrusions (Supplementary Figure 2b). In this study, a superficial calcific sheet, which was frequently located in the left anterior descending coronary artery, was the most prevalent type of lesion and was associated with the highest levels of post-PCI myocardial damage. However, this classification system has not been histologically validated.

Spontaneous coronary artery dissection. Spontaneous coronary artery dissection (SCAD) is an underdiagnosed condition that frequently affects middle-aged women without cardiovascular risk factors and can cause myocardial infarction and cardiac death[71]. The hallmark appearance of SCAD in OCT images is an accumulation of blood or flushing media within the medial space, displacing the IEM inwards and EEM outwards (intramural haematoma), with or without communication with the lumen (intimal tear) (FIG. 5e). Overlying thrombi are rarely observed in SCAD. OCT can provide greater diagnostic clarity than IVUS in assessing the distinctive features of intramural haematoma and intimal tear. However, the instrumentation and injection of contrast media into a dissected vessel carries the risk of propagation of dissection and vessel closure. Therefore, OCT imaging should be reserved for patients in whom diagnostic uncertainty persists, particularly angiographic SCAD types 3 and 4 (REF.[72]).

Myocardial infarction with non-obstructive coronary arteries. Myocardial infarction with non-obstructive coronary arteries (MINOCA) accounts for 6–15% of cases of spontaneous myocardial infarction and frequently affects women[73]. The pathogenesis of MINOCA is varied and includes vascular aetiologies, such as plaque rupture, erosion, vasospasm and embolization, SCAD or microvascular disease, for which findings are often angiographically inapparent. Incomplete understanding of the mechanisms of ACS leads to variable use of diagnostic testing and medical therapies for secondary prevention, with high costs and reduced efficacy. In the absence of clinically significant obstructive lesions on angiography, physicians should consider non-atherosclerotic aetiologies, particularly if patients present with atypical symptoms or unusual demographic or clinical risk profiles. OCT is an invaluable tool to detect atherosclerotic plaque disruption or non-atherosclerotic arterial pathology[74,75]. In the management of patients with MINOCA, targeted therapies based on underlying pathology identified by OCT, such as lipid-lowering therapy and potent antiplatelet therapy for atherosclerotic plaque disruption, are recommended[73].

Detection of vulnerable plaque

Detection of vulnerable plaque has been one of the main focuses of OCT research and can help to identify patients who will benefit from pre-emptive local treatment or aggressive preventative therapies such as PCSK9 inhibitors or anti-inflammatory therapies. In a retrospective study of OCT in 1,474 patients undergoing PCI, those with lipid-rich plaque had a higher incidence of major adverse cardiac events at 2 years than those without lipid-rich plaque (HR 2.06, 95% CI 1.05–4.04, $P=0.036$)[76]. However, repeat revascularization was the main driver of the primary end point of this study rather than cardiac death or myocardial infarction. In a post hoc analysis of this study, 174 TCFAs were identified and, among these, only 2 (1.1%) caused acute myocardial infarction during the 2-year follow-up[77]. The prospective CLIMA study[78] expanded the OCT-derived information, pursuing as a new goal the identification of simultaneous metrics of vulnerability. Four criteria (thin fibrous cap, large lipid arc, small lumen area and presence of OCT-detected macrophages) identified patients at risk of hard clinical events, including cardiac death or myocardial infarction[78]. In an observational study, non-culprit plaques characterized by OCT as both lipid-rich and TCFA were associated with an increased risk of subsequent ACS at the lesion level[79]. Data to support the use of interventional therapies for vulnerable plaques are currently absent. Studies testing the potential value of detecting vulnerable plaque as well as studies on the natural history of vulnerable plaque are warranted before the routine use of OCT imaging in this context can be recommended.

Serial OCT examination

Atherosclerosis was traditionally thought to be a disease of insidious onset and slow progress secondary to smooth muscle cell proliferation[80]. However, this concept has been challenged by the alternative paradigm of rapid, stepwise plaque progression[81]. This sudden change in the arterial lumen occurs when a mural thrombus is organized after destabilization of a plaque or by the sudden expansion of a plaque secondary to intraplaque haemorrhage. Plaque morphology changes dynamically, which could invalidate the use of OCT assessment at any single time point to predict future events. OCT can characterize microstructural details of the coronary wall and can therefore be used to evaluate the progression or regression of atheroma features such as plaque width and length, cap thickness, and macrophage and lumen area. Longitudinal studies (baseline versus follow-up) can be used to evaluate the progression or regression of coronary atherosclerosis and the response to medical treatment or stent implantation.

Serial images are co-registered using landmarks such as side branches, calcification, coronary ostia and stent edges. After co-registration, the plaques or stents are compared using qualitative or quantitative measurements. To achieve consistency across serial examinations, care should be taken to ensure optimal image quality and the use of the same OCT system, pullback speed and flushing medium. Given that OCT is an invasive procedure, it cannot be used as a screening tool, and clear justification is needed to perform serial OCT imaging. OCT cannot assess progression or regression of the atheroma thickness, area or volume when the EEM cannot be identified. Combining OCT with other imaging modalities, such as IVUS or near-infrared spectroscopy (NIRS), could help to characterize the plaque and obtain information on deep lesion components.

In a study of OCT findings of non-clinically significant coronary plaques that subsequently progressed at 6–9-month follow-up, OCT-defined TCFA and microvessels were associated with plaque progression[82]. Yamamoto et al. compared OCT findings at baseline and at 8-month follow-up and reported that OCT-defined layered patterns (indicative of clinically silent plaque rupture and healing) were involved in subsequent plaque progression[83]. In a study of serial observations of 517 lesions in 248 patients, OCT-defined lipid-rich plaque, TCFA and layered plaque were predictors of subsequent angiographic progression identified by angiography at 7-month follow-up[84]. Prospective OCT studies are warranted to better understand the mechanism of atheroma progression and regression.

Studies with PCSK9 inhibitors

An IVUS study demonstrated that PCSK9 inhibitors in combination with statins produce regression of coronary atherosclerosis, with the benefit proportional to the extent of LDL-cholesterol lowering[85]. OCT allows characterization of the plaque surface and individual components of the atheroma. Although OCT studies have demonstrated that statin therapy alone can increase fibrous cap thickness in patients with coronary artery disease[29,86], the effect of PCSK9 inhibition on plaque phenotype has not been clarified. An observational study demonstrated early increases in fibrous cap thickness and a reduction in lipid arc in patients treated with the combination of a statin and a PCSK9 inhibitor after ACS[87]. The prospective HUYGENS trial[88] (NCT03570697), which was completed in 2021, was

Abluminal
Away from the lumen.

designed to assess whether PCSK9 inhibition in addition to statin therapy favourably modifies coronary plaque phenotype.

OCT for optimization of PCI

OCT provides information that can be used to optimize stent implantation and minimize stent-related complications. In the non-randomized ILUMIEN I study[89], pre-stent OCT imaging changed the PCI strategy more frequently than with imaging performed after stent implantation (57% versus 27%, respectively). The size and length of the balloon and stent are decided on the basis of pre-PCI OCT measurements, which are more accurate than those obtained by quantitative coronary angiography. Plaque morphology should be assessed before treatment to guide lesion preparation and stent selection. For heavily calcified lesions, a debulking technique (such as atherectomy or intravascular lithotripsy) can be considered for better lesion preparation and to avoid underexpansion. OCT is valuable to confirm calcium fracture, which is associated with improved stent expansion[90]. When pre-dilatation or debulking has been performed, OCT imaging should be repeated to confirm sufficient lesion preparation and optimize stent size.

A normal segment of vessel (or near-normal segment in the case of a diffusely diseased artery) closest to the target lesion can be used as a landing zone for the stent. Given that the presence of lipid-rich plaque in the landing zone is associated with an increased risk of periprocedural myocardial infarction[91] and stent edge restenosis[92], landing in a lipid-rich area should be avoided. In the EAPCI document, the use of the mean distal lumen diameter with rounding-up the stent diameter (for example, 3.76 mm rounded to 4.00 mm) or the mean EEM (two orthogonal measurements) with rounding-down the stent diameter (for example, 3.76 mm rounded to 3.50 mm) is proposed[21]. Practical strategies for OCT-based optimization of PCI are detailed in the EAPCI document[21].

PCI-related findings

Basic stent measurements. Given that metal stent struts are opaque to light, only the luminal (leading) surface of individual struts is visualized by OCT. The following stent measurements can be made:

- Stent area: the area bounded by the stent border.
- Minimum stent diameter: the shortest diameter through the centre point of the stent.
- Maximum stent diameter: the longest diameter through the centre point of the stent.
- Stent eccentricity: the (maximum stent diameter minus the minimum stent diameter) divided by the maximum stent diameter in a cross-sectional image.
- Neointima burden: the (cross-sectional area of the stent minus the cross-sectional area of the lumen) divided by the cross-sectional area of the stent, assuming no malapposition.

Stent underexpansion. Stent expansion describes the minimum stent area (MSA) either as an absolute expansion (MSA itself) or a relative expansion (MSA divided by the mean of the proximal and distal reference lumen areas). A small MSA is known to be a predictor of suboptimal post-PCI fractional flow reserve (FFR)[93] and adverse outcomes[94,95]. Various targets of stent expansion have been adopted in clinical trials assessing the use of OCT-guided PCI[8,9,96]. In the EAPCI document, a relative expansion of >80% is the recommended target for stent optimization[21]. However, this recommendation is controversial because a relative expansion of >80% can result in a small MSA in small vessels. Calcification has been reported to be a major risk factor for stent underexpansion[20,21] as discussed in the section on calcified plaque in this Review.

Malapposition. OCT enables accurate assessment of apposition of stent struts to the arterial wall. If the axial distance between the surface of the strut and the luminal surface is greater than the strut thickness (including the polymer, if present), the strut is considered to be malapposed (FIG. 6a). Differences in strut thickness between different stents should be considered. OCT studies have reported that malapposition is associated with acute (<1 day), subacute (1–30 days), late (30 days to 1 year) and very late (>1 year) stent thrombosis[97,98]. However, malapposition noted at the time of stent thrombosis might either have been present after the index PCI (persistent malapposition) or have developed during follow-up (late-acquired malapposition) owing to thrombus resolution or vascular toxicity from the stent. Further studies are required to determine whether malapposition is an independent risk factor for stent thrombosis. Malapposition increases the risk of accidental abluminal rewiring and deformation of the stent in the aorto-ostial segment owing to collision with the guiding catheter. In the EAPCI document, correction of acute malapposition of <0.4 mm with longitudinal extension <1 mm is not recommended because spontaneous neointimal integration is anticipated[21].

Tissue prolapse. Tissue prolapse between stent struts towards the lumen can be caused by the protrusion of non-calcified plaque or, in the context of ACS, of atherothrombotic material (FIG. 6b). OCT enables clearer visualization of tissue prolapse than IVUS. Tissue prolapse is more frequently observed when the stent is placed over a lipid-rich plaque or TCFA. In patients with ACS, tissue prolapse has been reported to be a predictor of target-lesion revascularization[95,99]. Insufficient evidence exists to support further intervention in cases of tissue prolapse.

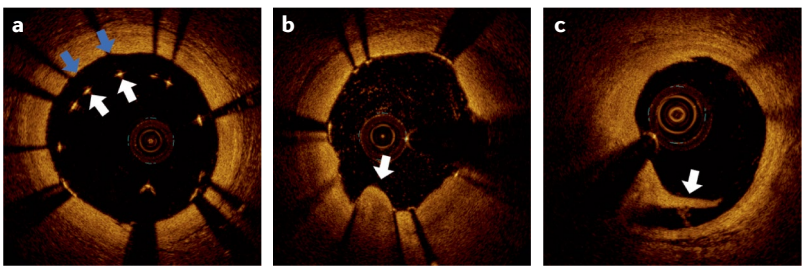

Fig. 6 | **Optical coherence tomography findings after percutaneous coronary intervention. a** | Strut malapposition; stent struts (white arrows) are distant from the luminal surface of the artery wall (blue arrows). **b** | Tissue prolapse; tissue extrusion from inside the stent area (arrow). **c** | Edge dissection (arrow).

Dissection. Edge dissections are tears of the luminal vessel surface that occur at the stent edge. OCT allows the visualization of subtle stent edge dissections typically missed on IVUS (FIG. 6c). In the ILUMIEN III: OPTIMIZE PCI study[8], edge dissections were classified as major when the dissection extended ≥60° of the circumference of the vessel or ≥3 mm in length. In the CLI-OPCI II study[94], distal edge dissection with a width ≥200 μm was a predictor of adverse events. By contrast, in a multicentre OCT registry, stent edge dissections were not associated with adverse events[95]. Minor edge dissections are unlikely to be clinically relevant[100,101]. Dissections can lead to intramural haematoma that sometimes progresses and can result in acute vessel closure, particularly when the haematoma is at the distal stent edge. In the EAPCI document, the following factors are recognized to increase the risk of adverse events: presence of residual plaque burden, extensive lateral (>60°) and longitudinal extension (>2 mm), involvement of deep vessel layers (medial or adventitia), and localization distal to the stent[21].

Comparative studies of OCT-guided PCI

OCT versus angiography. In the CLI-OPCI registry study[102], a reduced rate of cardiac death and major adverse cardiac events was reported in patients who underwent OCT-guided PCI compared with angiography-guided PCI (9.6% versus 14.8%; $P = 0.044$). Additional observational studies have shown that OCT-guided primary PCI is associated with increased final in-stent minimum lumen diameter[103] and a reduction in the number of stents used[104]. In the randomized DOCTORS trial[9], among 240 patients with non-ST-segment elevation ACS, OCT-guided PCI was associated with an improvement in post-procedural FFR compared with angiography-guided PCI (0.94 ± 0.04 versus 0.92 ± 0.05; $P = 0.005$). In the OCTACS study[96], which included 100 patients with ACS, OCT guidance resulted in a lower proportion of uncovered struts at 6 months compared with angiography guidance (4.3% versus 9.0%; $P < 0.01$). In the randomized DETECT OCT study[105], which included 894 patients with coronary artery disease, OCT guidance resulted in superior stent coverage at 3 months compared with angiography guidance (7.5% versus 9.9%; $P = 0.009$). In the observational Pan-London PCI registry[106] of 87,166 patients who underwent PCI, OCT-guided PCI was associated with improved procedural outcomes, reduced in-hospital events and improved long-term survival compared with standard angiography-guided PCI. In the randomized ILUMIEN III trial[8], OCT-guided, IVUS-guided and angiography-guided PCI were compared for stent expansion in 450 patients. OCT met the primary end point of non-inferiority compared with IVUS but was not found to be superior to angiography with respect to MSA. Nonetheless, OCT guidance led to improved relative stent expansion, fewer untreated dissections and a reduced rate of persistent major malapposition compared with angiography guidance. No significant differences in clinical outcomes at 1 year between the imaging modalities were reported in this low-risk patient population; however, this study was not powered for clinical outcomes[107]. The effect of OCT-guided versus angiography-guided PCI on clinical outcomes is being investigated in three randomized controlled trials that are under way: ILUMIEN IV[108] (NCT0350777), COCOA[109] (NCT03176810) and OCTOBER[110] for bifurcation lesions (NCT03171311). Published studies in which OCT-guided PCI was compared with angiography-guided PCI are summarized in Supplementary Table 1.

OCT versus IVUS. The randomized ILUMIEN III[107] and OPINION[7] trials consistently showed that OCT guidance is non-inferior to IVUS guidance with respect to the procedural result as well as for mid-term clinical outcomes. A meta-analysis of data from 17,882 patients who underwent stent implantation guided by angiography, IVUS or OCT in 17 randomized controlled trials and 14 observational studies demonstrated that IVUS and OCT were both associated with significant reductions in major adverse cardiac events and cardiovascular death compared with angiography, without significant differences between IVUS and OCT[111]. Currently, no data support the superiority of OCT over IVUS to improve clinical outcomes after PCI. Either modality can be used to identify features of optimal stent implantation (expansion and apposition) as well as complications and mechanisms of stent failure that cannot be captured using angiography alone. However, measurements of lumen area derived from OCT have been reported to be smaller than measurements derived from IVUS[10,112,113].

OCT versus physiology index. PCI for stable angina is indicated for haemodynamically significant coronary stenoses[114,115]. Pressure-derived indices are the accepted gold standard for invasive assessment of ischaemia[114,116]. A randomized trial that included angiographically intermediate stenosis demonstrated a lower occurrence of adverse events in OCT-guided PCI than in FFR-guided PCI[117]. The study was conducted at a single centre and included only 350 patients; therefore, further studies are required to replicate this finding. The effect of the addition of OCT to FFR on clinical outcomes is being investigated in the randomized COMBINE (OCT-FFR) trial[118] (NCT02989740). Several studies have reported that lumen measurements and plaque morphology assessed by OCT correlate with FFR[119]. A slight superiority of OCT over IVUS for the detection of FFR-positive lesions has been reported[120,121]. Optical flow ratio (OFR) is an OCT-based method for the functional assessment of coronary stenosis based on computational fluid dynamics. OFR showed excellent agreement with FFR and was superior to minimum lumen area in the detection of physiologically significant stenoses[122]. Post-PCI OFR showed good diagnostic concordance with post-PCI FFR[123]. Further studies on this topic are warranted.

OCT for bifurcation lesions. OCT provides useful guidance for the treatment of bifurcation lesions. OCT depicts an ostial lesion in bifurcation without overlap and foreshortening, which frequently occur on angiograms. 3D reconstruction can be used to understand the geometry and morphology of bifurcation lesions.

Computational fluid dynamics
A branch of fluid mechanics that uses numerical analysis and data structures to analyse and solve problems that involve fluid flows.

Contour
The boundary of a certain object, such as the lumen, stent or plaque component.

After stent implantation, OCT can guide the recrossing of guidewires through stent struts jailing the side branch ostium (Supplementary Figure 3) and confirm optimization of bifurcation segments. The clinical importance of this approach is being tested in the randomized OCTOBER trial[110] (NCT03171311). Another randomized trial demonstrated that 3D-OFDI guidance was superior to angiography guidance in terms of acute stent apposition at bifurcation[124]. In the LEMON study[125], the feasibility and performance of OCT-guided left main stem PCI according to a prespecified protocol was reported; OCT guidance modified the operator strategy in 26% of patients. The use of OCT for bifurcation lesions is detailed in the joint consensus statement from the European and Japanese bifurcation clubs[126].

Late stent change

Strut coverage. The low susceptibility of OCT to artefacts at the stent strut enables the visualization of tissue overlying the struts and the evaluation of the response to stent implantation. Struts are termed 'covered' if any tissue can be identified above the struts (FIG. 7a) and 'uncovered' if no evidence of tissue can be visualized above the struts (FIG. 7b). The coverage thickness can be measured as the distance between the adluminal surface of the covered tissue and the abluminal reflective edge of the metallic struts. The type of tissue (for example, fibrin, endothelium, thrombus or mature neointima) cannot be ascertained at present because a single-cell endothelial layer is beyond the limits of resolution of OCT. Tissue characteristics, such as backscattering intensity, can provide some discrimination of tissue type[127]. A threshold of tissue above struts of ≥40 μm was reported to help to detect healthy strut coverage[128]. However, this issue needs further investigation because the study was small ($n = 25$). In addition, whether the tissue that covers the struts is less thrombogenic than the strut or is non-thrombogenic is unknown. As with apposition, strut coverage can be reported per strut, per cross-section or per stent. The percentage of uncovered struts can be measured as the (number of struts without distinct overlying tissue, in which the luminal reflection of the strut surface is directly interfacing with the lumen, divided by the total number of analysable struts) multiplied by 100.

Evagination. Stent implantation, and the ensuing mechanical trauma and inflammatory reactions, can lead to vascular positive remodelling causing evagination. Evagination appears in OCT images as an outward bulge in the luminal vessel contour between apposed struts (FIG. 7c). In a retrospective study, evagination was more frequent in first-generation than in second-generation drug-eluting stents[129]. Further studies are needed to understand this finding.

Classification of neointima. OCT provides detailed morphological information about neointimal tissue within stents. Neointimal tissue has historically been subdivided into three different patterns by OCT: homogeneous, heterogeneous and layered (BOX 4). In a serial OCT study, neointimal patterns were reported to have changed between 6 months and 12 months in 11% of stents[130]. Further studies are needed to understand the mechanisms of these changes and their clinical importance. In a histopathology study, seven distinct neointimal patterns were identified from OCT images: homogeneous (45%), layered (15%), high intensity with high attenuation (14%), intraluminal protruding masses (8%), peri-strut low attenuation (7%), heterogeneous (2%) and honeycomb (1%)[131]. The homogeneous pattern correlated most often with smooth muscle cells within collagen–proteoglycan matrix and less often with organized thrombus. The layered pattern correlated with healed neointimal rupture or erosion, peri-strut neovascularization, or smooth muscle cells within collagen–proteoglycan matrix. High intensity with high attenuation correlated with superficial macrophage accumulation in the majority of cases but with other histological findings in 30% of cases[131]. Neointimal patterns might offer guidance for the treatment of in-stent restenosis[132], although this issue requires further investigation.

Neoatherosclerosis. Clinical trials have shown a continuous requirement for target-lesion revascularization over time, irrespective of the generation of the stent[133]. Atherosclerotic changes within the neointima have an important role in the development of stent-related adverse events. Neoatherosclerosis is defined by the presence of at least one of the components of a mature

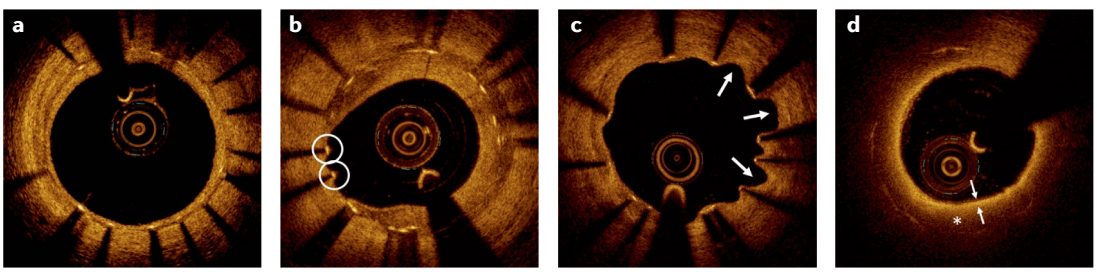

Fig. 7 | **Optical coherence tomography images of vascular response to stenting. a** | Covered struts; stent struts are considered covered when tissue can be identified on the luminal side of the strut. **b** | Uncovered struts; stent struts are considered uncovered when tissue cannot be identified above the strut (struts in white circles). **c** | Evagination; an outward bulge (arrows) in the luminal vessel contour between apposed struts. **d** | Neoatherosclerosis; a signal-poor region with a diffuse border (asterisk) and an overlying signal-rich band (arrows), which correspond with lipid-laden tissue, are seen within the stent.

Box 4 | **Classification of neointima by optical coherence tomography**

Homogeneous neointima

Homogeneous neointima has a uniform, signal-rich band without focal variation or attenuation (see the figure, panel **a**). This pattern is frequently observed in bare-metal stent neointima within 1 year of stenting and indicates stable, fibrous tissue.

Heterogeneous neointima

Heterogeneous neointima has focally changing optical properties and various backscattering patterns (see the figure, panel **b**). This pattern and layered neointima are frequently observed in drug-eluting stents and indicate the deposition of fibrin, platelets or extracellular matrix proteoglycans during the acute phase of implantation[151].

Layered neointima

Layered neointima has layers with different optical properties such as an adluminal high-scattering layer (yellow arrow) and an abluminal low-scattering layer (blue arrow)[152] (see the figure, panel **c**).

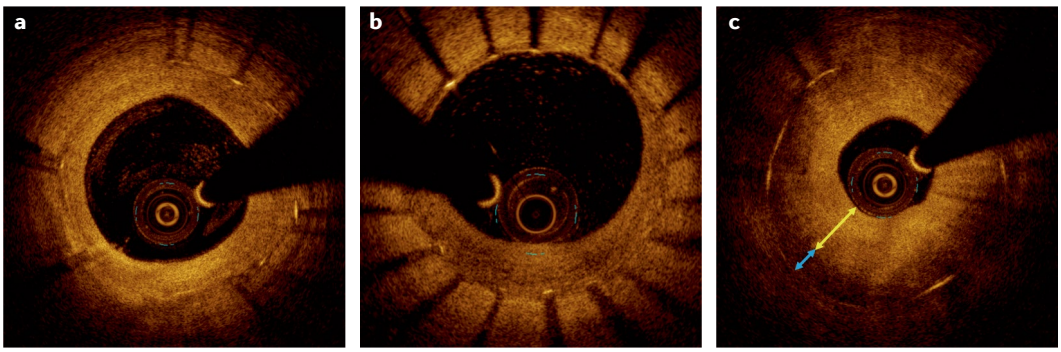

a | Homogeneous neointima. **b** | Heterogeneous neointima. **c** | Layered neointima.

atherosclerotic plaque such as lipid-laden tissue or calcification within the stent (FIG. 7d). OCT enables the detection of neoatherosclerosis in vivo. Neoatherosclerosis increases with time after stenting and appears earlier in drug-eluting than in bare-metal stents[134,135]. Neoatherosclerosis and subsequent disruption of lipid-laden neointima are known to be associated with very late stent thrombosis[97,98,136].

Cost-effectiveness of OCT

One common barrier to the widespread use of OCT is its high cost[137], which includes the imaging catheters, the introduction of the imaging system to the catheterization laboratory, training for staff and extended procedure time. Although IVUS-guided PCI is known to be more cost-effective than angiography-guided PCI[138,139], whether OCT-guided PCI is equally cost-effective as IVUS-guided PCI is not known. This issue requires study.

Limitations of OCT

Although OCT is a valuable imaging modality that has many clinical and research applications, limitations do exist. First, OCT light cannot penetrate objects that are highly backscattering or rapidly attenuating (such as blood, lipid, red thrombus and stent struts), precluding the assessment of underlying objects. Owing to its shallow penetration depth, OCT sometimes fails to visualize the entire circumference of the IEM or EEM. However, the assessment of plaque burden and vascular remodelling are not frequently used in clinical practice, and the OPINION trial[7] showed that lumen size in the reference segment can be used for the optimization of OCT-guided PCI. Second, the OCT catheter can potentially cause injury to the coronary artery. However, this complication was not observed in a prospective registry of 1,142 OCT procedures[5]. Third, contrast media needed for the clearance of blood can cause acute kidney injury. As described in the section of this Review on safety data, this complication is rare in patients without pre-existing chronic kidney disease. Other potential flushing media have been discussed in the section of this Review on OCT image acquisition. Fourth, OCT is associated with high costs, which are discussed in the preceding section on cost-effectiveness. Fifth, OCT imaging necessitates skills for correct acquisition and interpretation of images as well as knowledge of the currently available evidence. Sixth, data to support the superiority of OCT-guided PCI over IVUS-guided PCI are lacking. These limitations could hamper the universal adoption of OCT in research and clinical practice in the setting of coronary atherosclerosis.

Future directions

OCT as a research tool

With its unprecedented resolution, OCT provides new research opportunities. Assessment of detailed plaque structures at the microscopic level will improve our understanding of the pathobiology of individual plaque structures. Combining OCT data with the measurement of biomarkers will provide an improved understanding of the mechanism of coronary atherosclerosis. Serial OCT imaging can be used to perform mechanistic studies; however, because OCT is an invasive procedure, a clear justification for its use is required. Correlating OCT findings to patient data using artificial intelligence could help to identify patients at high risk of cardiac events.

Deep learning
A class of machine learning algorithm that uses multiple layers to progressively extract higher-level features from the raw input.

Fluorescence
The emission of light by a substance that has absorbed light or other electromagnetic radiation.

Polarization
A property of light described by the magnitude, orientation and precession of its electric field.

Birefringence
A phenomenon exhibited by a material in which light travelling through the material is divided into two beams of different polarizations.

Depolarization
When the incident beam is fully linearly or circularly polarized, the scattered light can become partially polarized or even totally unpolarized.

OCT as a clinical tool

Although several small studies have demonstrated a potential role for OCT in the optimization of PCI, no robust data exist to show the superiority of OCT over IVUS or angiography at improving clinical outcomes. The cost-effectiveness of OCT-guided PCI needs to be investigated. Automatic interpretation of images, such as of plaque erosion, would facilitate the widespread clinical use of OCT. Further studies that assess the value of OCT-based management in patients with ACS, secondary to plaque erosion or to MINOCA, are warranted.

Deep learning-aided OCT interpretation

Deep learning, which is a form of machine learning algorithm, has the potential to transform clinical care in medical imaging fields. Deep learning could aid the interpretation of OCT images such as tissue characterization and guidance in stent sizing and optimization[140–142]. However, currently available deep learning data in OCT interpretation are limited and have not been replicated. In addition, randomized studies assessing the benefit of deep learning-aided OCT interpretation are lacking.

New OCT imaging catheters

Hybrid OCT-based imaging, such as IVUS–OCT[143], OCT–NIRS[144], OCT–near-infrared fluorescence[145], OCT–fluorescence lifetime imaging microscopy[146], higher resolution OCT (micro-OCT)[147] and polarization-sensitive (PS) OCT[148], are being developed and could provide additional insights in the assessment of coronary atherosclerosis. IVUS–OCT could overcome the OCT limitation of the shallow penetration depth of light and enable the assessment of EEM in a lipid-rich plaque. OCT–NIRS could provide structural and chemical information that would be likely to improve the identification of lipid-rich plaque. OCT–near-infrared fluorescence utilizes photoluminescence to provide information on the molecular aspects of plaque, which is obtained using a mutual optical fibre and lens with OCT. OCT–fluorescence lifetime imaging microscopy measures a lifetime of autofluorescence signals, which are emitted from the excitation by ultraviolet light, and identifies cellular and molecular components of the plaque, including macrophages, lipoproteins, collagen and elastin. Micro-OCT, which has a spatial resolution of 1–2 μm, has the potential to identify the thin layer of endothelium. Polarization-sensitive OCT measures the birefringence and depolarization of tissue and could improve the characterization of plaques.

Conclusions

The rapid growth in publications on cardiac OCT over the past decade has provided new insights into the pathogenesis of atherogenesis and the pathobiology of ACS. However, various analytical methods and a lack of defined standards or criteria for OCT use and interpretation have resulted in inconsistent interpretation and conclusions. In this Review, we have summarized the latest knowledge and evidence from OCT research and clinical use in cardiology, particularly for the in vivo diagnosis of plaque erosion, healed coronary plaque, neoatherosclerosis and MINOCA, and for the optimization of PCI. In addition, we have proposed standards that can be used in future OCT research and clinical application.

Published online 21 April 2022

1. Huang, D. et al. Optical coherence tomography. *Science* **254**, 1178–1181 (1991).
2. Jang, I. K. et al. Visualization of coronary atherosclerotic plaques in patients using optical coherence tomography: comparison with intravascular ultrasound. *J. Am. Coll. Cardiol.* **39**, 604–609 (2002).
3. Yabushita, H. et al. Characterization of human atherosclerosis by optical coherence tomography. *Circulation* **106**, 1640–1645 (2002).
4. Tearney, G. J. et al. Consensus standards for acquisition, measurement, and reporting of intravascular optical coherence tomography studies: a report from the International Working Group for Intravascular Optical Coherence Tomography Standardization and Validation. *J. Am. Coll. Cardiol.* **59**, 1058–1072 (2012).
5. van der Sijde, J. N. et al. Safety of optical coherence tomography in daily practice: a comparison with intravascular ultrasound. *Eur. Heart J. Cardiovasc. Imaging* **18**, 467–474 (2017).
6. Terada, N. et al. Ventricular fibrillation during optical coherence tomography/optical frequency domain imaging — a large single-center experience. *Circ. J.* **84**, 178–185 (2020).
7. Kubo, T. et al. Optical frequency domain imaging vs. intravascular ultrasound in percutaneous coronary intervention (OPINION trial): one-year angiographic and clinical results. *Eur. Heart J.* **38**, 3139–3147 (2017).
8. Ali, Z. A. et al. Optical coherence tomography compared with intravascular ultrasound and with angiography to guide coronary stent implantation (ILUMIEN III: OPTIMIZE PCI): a randomised controlled trial. *Lancet* **388**, 2618–2628 (2016).
9. Meneveau, N. et al. Optical coherence tomography to optimize results of percutaneous coronary intervention in patients with non-st-elevation acute coronary syndrome: results of the multicenter, randomized DOCTORS Study (Does Optical Coherence Tomography Optimize Results of Stenting). *Circulation* **134**, 906–917 (2016).
10. Kubo, T. et al. OCT compared with IVUS in a coronary lesion assessment: the OPUS-CLASS study. *JACC Cardiovasc. Imaging* **6**, 1095–1104 (2013).
11. Gerbaud, E. et al. Multi-laboratory inter-institute reproducibility study of IVOCT and IVUS assessments using published consensus document definitions. *Eur. Heart J. Cardiovasc. Imaging* **17**, 756–764 (2016).
12. Terashima, M. et al. Accuracy and reproducibility of stent-strut thickness determined by optical coherence tomography. *J. Invasive Cardiol.* **21**, 602–605 (2009).
13. Kini, A. S. et al. Fibrous cap thickness by optical coherence tomography in vivo. *J. Am. Coll. Cardiol.* **69**, 644–657 (2017).
14. Radu, M. D. et al. Variability in the measurement of minimum fibrous cap thickness and reproducibility of fibroatheroma classification by optical coherence tomography using manual versus semi-automatic assessment. *EuroIntervention* **12**, e987–e997 (2016).
15. Galon, M. Z. et al. Differences determined by optical coherence tomography volumetric analysis in non-culprit lesion morphology and inflammation in ST-segment elevation myocardial infarction and stable angina pectoris patients. *Catheter. Cardiovasc. Interv.* **85**, E108–E115 (2015).
16. Tuzcu, E. M. et al. High prevalence of coronary atherosclerosis in asymptomatic teenagers and young adults: evidence from intravascular ultrasound. *Circulation* **103**, 2705–2710 (2001).
17. Kume, T. et al. Assessment of the coronary calcification by optical coherence tomography. *EuroIntervention* **6**, 768–772 (2011).
18. Saita, T. et al. Histopathological validation of optical frequency domain imaging to quantify various types of coronary calcifications. *Eur. Heart J. Cardiovasc. Imaging* **18**, 342–349 (2017).
19. Ong, D. S. et al. Coronary calcification and plaque vulnerability: an optical coherence tomographic study. *Circ. Cardiovasc. Imaging* **9**, e003929 (2016).
20. Fujino, A. et al. A new optical coherence tomography-based calcium scoring system to predict stent underexpansion. *EuroIntervention* **13**, e2182–e2189 (2018).
21. Raber, L. et al. Clinical use of intracoronary imaging. Part 1: guidance and optimization of coronary interventions. An expert consensus document of the European Association of Percutaneous Cardiovascular Interventions. *Eur. Heart J.* **39**, 3281–3300 (2018).
22. Kawasaki, M. et al. Diagnostic accuracy of optical coherence tomography and integrated backscatter intravascular ultrasound images for tissue characterization of human coronary plaques. *J. Am. Coll. Cardiol.* **48**, 81–88 (2006).
23. Kato, K. et al. Nonculprit plaques in patients with acute coronary syndromes have more vulnerable features compared with those with non-acute coronary syndromes: a 3-vessel optical coherence tomography study. *Circ. Cardiovasc. Imaging* **5**, 433–440 (2012).
24. Vergallo, R. et al. Prevalence and predictors of multiple coronary plaque ruptures: in vivo 3-vessel optical coherence tomography imaging study. *Arterioscler. Thromb. Vasc. Biol.* **36**, 2229–2238 (2016).
25. Virmani, R., Burke, A. P., Farb, A. & Kolodgie, F. D. Pathology of the vulnerable plaque. *J. Am. Coll. Cardiol.* **47**, C13–C18 (2006).
26. Yonetsu, T. et al. In vivo critical fibrous cap thickness for rupture-prone coronary plaques assessed by optical coherence tomography. *Eur. Heart J.* **32**, 1251–1259 (2011).
27. Tearney, G. J. et al. Quantification of macrophage content in atherosclerotic plaques by optical coherence tomography. *Circulation* **107**, 113–119 (2003).
28. Raber, L. et al. Changes in coronary plaque composition in patients with acute myocardial infarction treated with high-intensity statin therapy (IBIS-4): a serial optical coherence tomography study. *JACC Cardiovasc. Imaging* **12**, 1518–1528 (2018).

29. Komukai, K. et al. Effect of atorvastatin therapy on fibrous cap thickness in coronary atherosclerotic plaque as assessed by optical coherence tomography: the EASY-FIT study. *J. Am. Coll. Cardiol.* **64**, 2207–2217 (2014).
30. Kolodgie, F. D. et al. Intraplaque hemorrhage and progression of coronary atheroma. *N. Engl. J. Med.* **349**, 2316–2325 (2003).
31. Kume, T. et al. Detection of plaque neovascularization by optical coherence tomography: ex vivo feasibility study and in vivo observation in patients with angina pectoris. *J. Invasive Cardiol.* **28**, 17–22 (2016).
32. Nishimiya, K. et al. In vivo visualization of adventitial vasa vasorum of the human coronary artery on optical frequency domain imaging. *Valid. Study Circ. J.* **78**, 2516–2518 (2014).
33. Aoki, T. et al. Evaluation of coronary adventitial vasa vasorum using 3D optical coherence tomography — animal and human studies. *Atherosclerosis* **239**, 203–208 (2015).
34. Abela, G. S. & Aziz, K. Cholesterol crystals rupture biological membranes and human plaques during acute cardiovascular events — a novel insight into plaque rupture by scanning electron microscopy. *Scanning* **28**, 1–10 (2006).
35. Crea, F. & Liuzzo, G. Pathogenesis of acute coronary syndromes. *J. Am. Coll. Cardiol.* **61**, 1–11 (2013).
36. Katayama, Y. et al. Feasibility and clinical significance of in vivo cholesterol crystal detection using optical coherence tomography. *Arterioscler. Thromb. Vasc. Biol.* **40**, 220–229 (2020).
37. Jinnouchi, H. et al. Detection of cholesterol crystals by optical coherence tomography. *EuroIntervention* **16**, 395–403 (2020).
38. Kang, S. J. et al. OCT findings in patients with recanalization of organized thrombi in coronary arteries. *JACC Cardiovasc. Imaging* **5**, 725–732 (2012).
39. Souteyrand, G. et al. Diagnosis and management of spontaneously recanalized coronary thrombus guided by optical coherence tomography — lessons from the French "Lotus Root" Registry. *Circ. J.* **82**, 783–790 (2018).
40. Prati, F. et al. Expert review document. Part 2: methodology, terminology and clinical applications of optical coherence tomography for the assessment of interventional procedures. *Eur. Heart J.* **33**, 2513–2520 (2012).
41. Kajander, O. A. et al. Feasibility and repeatability of optical coherence tomography measurements of pre-stent thrombus burden in patients with STEMI treated with primary PCI. *Eur. Heart J. Cardiovasc. Imaging* **16**, 96–107 (2015).
42. Burke, A. P. et al. Healed plaque ruptures and sudden coronary death: evidence that subclinical rupture has a role in plaque progression. *Circulation* **103**, 934–940 (2001).
43. Mann, J. & Davies, M. J. Mechanisms of progression in native coronary artery disease: role of healed plaque disruption. *Heart* **82**, 265–268 (1999).
44. Otsuka, F., Joner, M., Prati, F., Virmani, R. & Narula, J. Clinical classification of plaque morphology in coronary disease. *Nat. Rev. Cardiol.* **11**, 379–389 (2014).
45. Vergallo, R. & Crea, F. Atherosclerotic plaque healing. *N. Engl. J. Med.* **383**, 846–857 (2020).
46. Shimokado, A. et al. In vivo optical coherence tomography imaging and histopathology of healed coronary plaques. *Atherosclerosis* **275**, 35–42 (2018).
47. Hoshino, M. et al. Optical coherence tomographic features of unstable coronary lesions corresponding to histopathological intraplaque hemorrhage evaluated by directional coronary atherectomy specimens. *JACC Cardiovasc. Interv.* **11**, 1414–1415 (2018).
48. Antuna, P. et al. Diagnosis of intraplaque hemorrhage by high-definition intravascular ultrasound and optical coherence tomography. *JACC Cardiovasc. Interv.* **13**, 1960–1962 (2020).
49. Pollack, A., Nazif, T., Mancini, D. & Weisz, G. Detection and imaging of cardiac allograft vasculopathy. *JACC Cardiovasc. Imaging* **6**, 613–623 (2013).
50. Cassar, A. et al. Coronary atherosclerosis with vulnerable plaque and complicated lesions in transplant recipients: new insight into cardiac allograft vasculopathy by optical coherence tomography. *Eur. Heart J.* **34**, 2610–2617 (2013).
51. Dong, L. et al. Optical coherence tomographic evaluation of transplant coronary artery vasculopathy with correlation to cellular rejection. *Circ. Cardiovasc. Interv.* **7**, 199–206 (2014).
52. Shan, P. et al. Comparison between cardiac allograft vasculopathy and native coronary atherosclerosis by optical coherence tomography. *Am. J. Cardiol.* **117**, 1361–1368 (2016).
53. Ichibori, Y. et al. Optical coherence tomography and intravascular ultrasound evaluation of cardiac allograft vasculopathy with and without intimal neovascularization. *Eur. Heart J. Cardiovasc. Imaging* **17**, 51–58 (2016).
54. Clemmensen, T. S. et al. Layered fibrotic plaques are the predominant component in cardiac allograft vasculopathy: systematic findings and risk stratification by OCT. *JACC Cardiovasc. Imaging* **10**, 773–784 (2017).
55. Clemmensen, T. S. et al. Detection of early changes in the coronary artery microstructure after heart transplantation: a prospective optical coherence tomography study. *J. Heart Lung Transpl.* **37**, 486–495 (2018).
56. Gerbaud, E. et al. Plaque burden can be assessed using intravascular optical coherence tomography and a dedicated automated processing algorithm: a comparison study with intravascular ultrasound. *Eur. Heart J. Cardiovasc. Imaging* **21**, 640–652 (2019).
57. Ramasamy, A. et al. Efficacy and reproducibility of attenuation-compensated optical coherence tomography for assessing external elastic membrane border and plaque composition in native and stented segments- an in vivo and histology-based study. *Circ. J.* **84**, 91–100 (2019).
58. Virmani, R., Kolodgie, F. D., Burke, A. P., Farb, A. & Schwartz, S. M. Lessons from sudden coronary death: a comprehensive morphological classification scheme for atherosclerotic lesions. *Arterioscler. Thromb. Vasc. Biol.* **20**, 1262–1275 (2000).
59. Partida, R. A., Libby, P., Crea, F. & Jang, I. K. Plaque erosion: a new in vivo diagnosis and a potential major shift in the management of patients with acute coronary syndromes. *Eur. Heart J.* **39**, 2070–2076 (2018).
60. Arbustini, E. et al. Plaque erosion is a major substrate for coronary thrombosis in acute myocardial infarction. *Heart* **82**, 269–272 (1999).
61. Higuma, T. et al. A combined optical coherence tomography and intravascular ultrasound study on plaque rupture, plaque erosion, and calcified nodule in patients with st-segment elevation myocardial infarction: incidence, morphologic characteristics, and outcomes after percutaneous coronary intervention. *JACC Cardiovasc. Interv.* **8**, 1166–1176 (2015).
62. Jia, H. et al. In vivo diagnosis of plaque erosion and calcified nodule in patients with acute coronary syndrome by intravascular optical coherence tomography. *J. Am. Coll. Cardiol.* **62**, 1748–1758 (2013).
63. Prati, F. et al. OCT-based diagnosis and management of STEMI associated with intact fibrous cap. *JACC Cardiovasc. Imaging* **6**, 283–287 (2013).
64. Jia, H. et al. Effective anti-thrombotic therapy without stenting: intravascular optical coherence tomography-based management in plaque erosion (the EROSION study). *Eur. Heart J.* **38**, 792–800 (2017).
65. Xing, L. et al. EROSION study (Effective Anti-Thrombotic Therapy Without Stenting: Intravascular Optical Coherence Tomography-Based Management in Plaque Erosion): a 1-year follow-up report. *Circ. Cardiovasc. Interv.* **10**, e005860 (2017).
66. Luping, H. et al. Predictors of non-stenting strategy for acute coronary syndrome caused by plaque erosion: 4-year outcomes of the EROSION study. *EuroIntervention* **17**, 497–505 (2020).
67. Combaret, N. et al. Management of ST-elevation myocardial infarction in young patients by limiting implantation of durable intracoronary devices and guided by optical frequency domain imaging: "proof of concept" study. *EuroIntervention* **13**, 397–406 (2017).
68. Torii, S. et al. Eruptive calcified nodules as a potential mechanism of acute coronary thrombosis and sudden death. *J. Am. Coll. Cardiol.* **77**, 1599–1611 (2021).
69. Kobayashi, N. et al. Features and outcomes of patients with calcified nodules at culprit lesions of acute coronary syndrome: an optical coherence tomography study. *Cardiology* **139**, 90–100 (2018).
70. Sugiyama, T. et al. Calcified plaques in patients with acute coronary syndromes. *JACC Cardiovasc. Interv.* **12**, 531–540 (2019).
71. Saw, J. et al. Canadian spontaneous coronary artery dissection cohort study: in-hospital and 30-day outcomes. *Eur. Heart J.* **40**, 1188–1197 (2019).
72. Saw, J. Coronary angiogram classification of spontaneous coronary artery dissection. *Catheter. Cardiovasc. Interv.* **84**, 1115–1122 (2014).
73. Tamis-Holland, J. E. et al. Contemporary diagnosis and management of patients with myocardial infarction in the absence of obstructive coronary artery disease: a scientific statement from the American Heart Association. *Circulation* **139**, e891–e908 (2019).
74. Gerbaud, E. et al. OCT and CMR for the diagnosis of patients presenting with MINOCA and Suspected epicardial causes. *JACC Cardiovasc. Imaging* **13**, 2619–2631 (2020).
75. Reynolds, H. R. et al. Coronary optical coherence tomography and cardiac magnetic resonance imaging to determine underlying causes of myocardial infarction with nonobstructive coronary arteries in women. *Circulation* **143**, 624–640 (2021).
76. Xing, L. et al. Clinical significance of lipid-rich plaque detected by optical coherence tomography: a 4-year follow-up study. *J. Am. Coll. Cardiol.* **69**, 2502–2513 (2017).
77. Jang, I. K. Pursuit for the detection of vulnerable plaque. *Eur. Heart J.* **41**, 392–393 (2020).
78. Prati, F. et al. Relationship between coronary plaque morphology of the left anterior descending artery and 12 months clinical outcome: the CLIMA study. *Eur. Heart J.* **41**, 383–391 (2019).
79. Kubo, T. et al. Optical coherence tomography detection of vulnerable plaques at high risk of developing acute coronary syndrome. *Eur. Heart J. Cardiovasc. Imaging* https://doi.org/10.1093/ehjci/jeab028 (2021).
80. Ross, R. The pathogenesis of atherosclerosis — an update. *N. Engl. J. Med.* **314**, 488–500 (1986).
81. Jang, I. K. Plaque progression slow linear or rapid stepwise? *Circ. Cardiovasc. Imaging* **314**, 488–500 (2017).
82. Uemura, S. et al. Thin-cap fibroatheroma and microchannel findings in optical coherence tomography correlate with subsequent progression of coronary atheromatous plaques. *Eur. Heart J.* **33**, 78–85 (2012).
83. Yamamoto, M. H. et al. Serial 3-vessel optical coherence tomography and intravascular ultrasound analysis of changing morphologies associated with lesion progression in patients with stable angina pectoris. *Circ. Cardiovasc. Imaging* **10**, e006347 (2017).
84. Araki, M. et al. Predictors of rapid plaque progression: an optical coherence tomography study. *JACC Cardiovasc. Imaging* **14**, 1628–1638 (2021).
85. Nicholls, S. J. et al. Effect of evolocumab on progression of coronary disease in statin-treated patients: the GLAGOV randomized clinical trial. *JAMA* **316**, 2373–2384 (2016).
86. Hattori, K. et al. Impact of statin therapy on plaque characteristics as assessed by serial OCT, grayscale and integrated backscatter-IVUS. *JACC Cardiovasc. Imaging* **5**, 169–177 (2012).
87. Yano, H., Horinaka, S. & Ishimitsu, T. Effect of evolocumab therapy on coronary fibrous cap thickness assessed by optical coherence tomography in patients with acute coronary syndrome. *J. Cardiol.* **75**, 289–295 (2019).
88. Nicholls, S. J. et al. Assessing the impact of PCSK9 inhibition on coronary plaque phenotype with optical coherence tomography: rationale and design of the randomized, placebo-controlled HUYGENS study. *Cardiovasc. Diagn. Ther.* **11**, 120–129 (2021).
89. Wijns, W. et al. Optical coherence tomography imaging during percutaneous coronary intervention impacts physician decision-making: ILUMIEN I study. *Eur. Heart J.* **36**, 3346–3355 (2015).
90. Kubo, T. et al. Superficial calcium fracture after PCI as assessed by OCT. *JACC Cardiovasc. Imaging* **8**, 1228–1229 (2015).
91. Imola, F. et al. Association between proximal stent edge positioning on atherosclerotic plaques containing lipid pools and postprocedural myocardial infarction (from the CLI-POOL Study). *Am. J. Cardiol.* **111**, 526–531 (2013).
92. Ino, Y. et al. Optical coherence tomography predictors for edge restenosis after everolimus-eluting stent implantation. *Circ. Cardiovasc. Interv.* **9**, e004231 (2016).
93. Belguidoum, S. et al. Relationship between stent expansion and fractional flow reserve after percutaneous coronary intervention: a post hoc analysis of the DOCTORS trial. *EuroIntervention* **17**, e132–e139 (2021).

94. Prati, F. et al. Clinical impact of OCT findings during PCI: the CLI-OPCI II study. *JACC Cardiovasc. Imaging* **8**, 1297–1305 (2015).
95. Soeda, T. et al. Incidence and clinical significance of poststent optical coherence tomography findings: one-year follow-up study from a multicenter registry. *Circulation* **132**, 1020–1029 (2015).
96. Antonsen, L. et al. Optical coherence tomography guided percutaneous coronary intervention with Nobori stent implantation in patients with non-st-segment-elevation myocardial infarction (OCTACS) trial: difference in strut coverage and dynamic malapposition patterns at 6 months. *Circ. Cardiovasc. Interv.* **8**, e002446 (2015).
97. Adriaenssens, T. et al. Optical coherence tomography findings in patients with coronary stent thrombosis: a report of the PRESTIGE Consortium (Prevention of Late Stent Thrombosis by an Interdisciplinary Global European Effort). *Circulation* **136**, 1007–1021 (2017).
98. Souteyrand, G. et al. Mechanisms of stent thrombosis analysed by optical coherence tomography: insights from the national PESTO French registry. *Eur. Heart J.* **37**, 1208–1216 (2016).
99. Prati, F. et al. Clinical impact of suboptimal stenting and residual intrastent plaque/thrombus protrusion in patients with acute coronary syndrome: the CLI-OPCI ACS substudy (Centro per la Lotta Contro L'Infarto-Optimization of Percutaneous Coronary Intervention in Acute Coronary Syndrome). *Circ. Cardiovasc. Interv.* **9**, e003726 (2016).
100. Kawamori, H. et al. Natural consequence of post-intervention stent malapposition, thrombus, tissue prolapse, and dissection assessed by optical coherence tomography at mid-term follow-up. *Eur. Heart J. Cardiovasc. Imaging* **14**, 865–875 (2013).
101. Radu, M. D. et al. Natural history of optical coherence tomography-detected non-flow-limiting edge dissections following drug-eluting stent implantation. *EuroIntervention* **9**, 1085–1094 (2014).
102. Prati, F. et al. Angiography alone versus angiography plus optical coherence tomography to guide decision-making during percutaneous coronary intervention: the Centro per la Lotta contro l'Infarto-Optimisation of Percutaneous Coronary Intervention (CLI-OPCI) study. *EuroIntervention* **8**, 823–829 (2012).
103. Sheth, T. N. et al. Optical coherence tomography-guided percutaneous coronary intervention in st-segment-elevation myocardial infarction: a prospective propensity-matched cohort of the thrombectomy versus percutaneous coronary intervention alone trial. *Circ. Cardiovasc. Interv.* **9**, e003414 (2016).
104. Iannaccone, M. et al. Impact of an optical coherence tomography guided approach in acute coronary syndromes: a propensity matched analysis from the international FORMIDABLE-CARDIOGROUP IV and USZ registry. *Catheter. Cardiovasc. Interv.* **90**, E46–E52 (2017).
105. Lee, S. Y. et al. early strut coverage in patients receiving drug-eluting stents and its implications for dual antiplatelet therapy: a randomized trial. *JACC Cardiovasc. Imaging* **11**, 1810–1819 (2018).
106. Jones, D. A. et al. Angiography alone versus angiography plus optical coherence tomography to guide percutaneous coronary intervention: outcomes from the Pan-London PCI Cohort. *JACC Cardiovasc. Interv.* **11**, 1313–1321 (2018).
107. Ali, Z. A. et al. Outcomes of optical coherence tomography compared with intravascular ultrasound and with angiography to guide coronary stent implantation: one-year results from the ILUMIEN III: OPTIMIZE PCI trial. *EuroIntervention* **16**, 1085–1091 (2021).
108. Ali, Z. et al. Optical coherence tomography-guided coronary stent implantation compared to angiography: a multicentre randomised trial in PCI - design and rationale of ILUMIEN IV: OPTIMAL PCI. *EuroIntervention* **16**, 1092–1099 (2021).
109. Kubo, T. et al. Comparison between optical coherence tomography guidance and angiography guidance in percutaneous coronary intervention (COCOA): study protocol for a randomized controlled trial. *J. Cardiol.* **72**, 170–175 (2018).
110. Holm, N. R. et al. Rational and design of the European randomized Optical Coherence Tomography Optimized Bifurcation Event Reduction Trial (OCTOBER). *Am. Heart J.* **205**, 97–109 (2018).
111. Buccheri, S. et al. Clinical outcomes following intravascular imaging-guided versus coronary angiography-guided percutaneous coronary intervention with stent implantation: a systematic review and bayesian network meta-analysis of 31 studies and 17,882 patients. *JACC Cardiovasc. Interv.* **10**, 2488–2498 (2017).
112. Bezerra, H. G. et al. Optical coherence tomography versus intravascular ultrasound to evaluate coronary artery disease and percutaneous coronary intervention. *JACC Cardiovasc. Interv.* **6**, 228–236 (2013).
113. Okamura, T. et al. First-in-man evaluation of intravascular optical frequency domain imaging (OFDI) of Terumo: a comparison with intravascular ultrasound and quantitative coronary angiography. *EuroIntervention* **6**, 1037–1045 (2011).
114. Neumann, F. J. et al. 2018 ESC/EACTS Guidelines on myocardial revascularization. *Eur. Heart J.* **40**, 87–165 (2019).
115. Fihn, S. D. et al. 2012 ACCF/AHA/ACP/AATS/PCNA/SCAI/STS guideline for the diagnosis and management of patients with stable ischemic heart disease: a report of the American College of Cardiology Foundation/American Heart Association Task Force on Practice Guidelines, and the American College of Physicians, American Association for Thoracic Surgery, Preventive Cardiovascular Nurses Association, Society for Cardiovascular Angiography and Interventions, and Society of Thoracic Surgeons. *J. Am. Coll. Cardiol.* **60**, e44–e164 (2012).
116. Patel, M. R. et al. ACC/AATS/AHA/ASE/ASNC/SCAI/SCCT/STS 2017 appropriate use criteria for coronary revascularization in patients with stable ischemic heart disease: a report of the American College of Cardiology Appropriate Use Criteria Task Force, American Association for Thoracic Surgery, American Heart Association, American Society of Echocardiography, American Society of Nuclear Cardiology, Society for Cardiovascular Angiography and Interventions, Society of Cardiovascular Computed Tomography, and Society of Thoracic Surgeons. *J. Am. Coll. Cardiol.* **69**, 2212–2241 (2017).
117. Burzotta, F. et al. Fractional flow reserve or optical coherence tomography to guide management of angiographically intermediate coronary stenosis: a single-center trial. *JACC Cardiovasc. Interv.* **13**, 49–58 (2020).
118. Kennedy, M. W. et al. Combined optical coherence tomography morphologic and fractional flow reserve hemodynamic assessment of non- culprit lesions to better predict adverse event outcomes in diabetes mellitus patients: COMBINE (OCT-FFR) prospective study. Rationale and design. *Cardiovasc. Diabetol.* **15**, 144 (2016).
119. Burzotta, F. et al. Correlation between frequency-domain optical coherence tomography and fractional flow reserve in angiographically-intermediate coronary lesions. *Int. J. Cardiol.* **253**, 55–60 (2018).
120. Usui, E. et al. Efficacy of optical coherence tomography-derived morphometric assessment in predicting the physiological significance of coronary stenosis: head-to-head comparison with intravascular ultrasound. *EuroIntervention* **13**, e2210–e2218 (2018).
121. Ramasamy, A. et al. Optical coherence tomography enables more accurate detection of functionally significant intermediate non-left main coronary artery stenoses than intravascular ultrasound: a meta-analysis of 6919 patients and 7537 lesions. *Int. J. Cardiol.* **301**, 226–234 (2020).
122. Huang, J. et al. Diagnostic performance of intracoronary optical coherence tomography-based versus angiography-based fractional flow reserve for the evaluation of coronary lesions. *EuroIntervention* **16**, 568–576 (2020).
123. Ding, D. et al. Optical Flow ratio for assessing stenting result and physiological significance of residual disease. *EuroIntervention* **17**, e989–e998 (2021).
124. Onuma, Y. et al. A randomized trial evaluating online 3-dimensional optical frequency domain imaging-guided percutaneous coronary intervention in bifurcation lesions. *Circ. Cardiovasc. Interv.* **13**, e009183 (2020).
125. Amabile, N. et al. Optical coherence tomography to guide percutaneous coronary intervention of the left main coronary artery: the LEMON study. *EuroIntervention* **17**, e124–e131 (2021).
126. Onuma, Y. et al. Joint consensus on the use of OCT in coronary bifurcation lesions by the European and Japanese bifurcation clubs. *EuroIntervention* **14**, e1568–e1577 (2019).
127. Templin, C. et al. Coronary optical frequency domain imaging (OFDI) for in vivo evaluation of stent healing: comparison with light and electron microscopy. *Eur. Heart J.* **31**, 1792–1801 (2010).
128. Jinnouchi, H. et al. Healthy strut coverage after coronary stent implantation: an ex vivo human autopsy study. *Circ. Cardiovasc. Interv.* **13**, e008869 (2020).
129. Radu, M. D. et al. Coronary evaginations are associated with positive vessel remodelling and are nearly absent following implantation of newer-generation drug-eluting stents: an optical coherence tomography and intravascular ultrasound study. *Eur. Heart J.* **35**, 795–807 (2014).
130. Yamamoto, E. et al. Dynamic neointimal pattern after drug-eluting stent implantation defined by optical coherence tomography. *Coron. Artery Dis.* **28**, 557–563 (2017).
131. Lutter, C. et al. Histopathological differential diagnosis of optical coherence tomographic image interpretation after stenting. *JACC Cardiovasc. Interv.* **9**, 2511–2523 (2016).
132. Xhepa, E. et al. Clinical outcomes by optical characteristics of neointima and treatment modality in patients with coronary in-stent restenosis. *EuroIntervention* **17**, e388–e395 (2020).
133. Madhavan, M. V. et al. Stent-related adverse events >1 year after percutaneous coronary intervention. *J. Am. Coll. Cardiol.* **75**, 590–604 (2020).
134. Takano, M. et al. Appearance of lipid-laden intima and neovascularization after implantation of bare-metal stents extended late-phase observation by intracoronary optical coherence tomography. *J. Am. Coll. Cardiol.* **55**, 26–32 (2009).
135. Nakazawa, G. et al. The pathology of neoatherosclerosis in human coronary implants bare-metal and drug-eluting stents. *J. Am. Coll. Cardiol.* **57**, 1314–1322 (2011).
136. Taniwaki, M. et al. Mechanisms of very late drug-eluting stent thrombosis assessed by optical coherence tomography. *Circulation* **133**, 650–660 (2016).
137. Koskinas, K. C. et al. Current use of intracoronary imaging in interventional practice — results of a European Association of Percutaneous Cardiovascular Interventions (EAPCI) and Japanese Association of Cardiovascular Interventions and Therapeutics (CVIT) Clinical Practice Survey. *EuroIntervention* **14**, e475–e484 (2018).
138. Zhou, J. et al. Intravascular ultrasound versus angiography-guided drug-eluting stent implantation: a health economic analysis. *Circ. Cardiovasc. Qual. Outcomes* **14**, e006789 (2021).
139. Alberti, A. et al. Understanding the economic impact of intravascular ultrasound (IVUS). *Eur. J. Health Econ.* **17**, 185–193 (2016).
140. Min, H. S. et al. Detection of optical coherence tomography-defined thin-cap fibroatheroma in the coronary artery using deep learning. *EuroIntervention* **16**, 404–412 (2019).
141. Chu, M. et al. Artificial intelligence and optical coherence tomography for the automatic characterisation of human atherosclerotic plaques. *EuroIntervention* **17**, 41–50 (2021).
142. Shibutani, H. et al. Automated classification of coronary atherosclerotic plaque in optical frequency domain imaging based on deep learning. *Atherosclerosis* **328**, 100–105 (2021).
143. Yin, J. et al. Integrated intravascular optical coherence tomography ultrasound imaging system. *J. Biomed. Opt.* **15**, 010512 (2010).
144. Fard, A. M. et al. Optical coherence tomography — near infrared spectroscopy system and catheter for intravascular imaging. *Opt. Express* **21**, 30849–30858 (2013).
145. Yoo, H. et al. Intra-arterial catheter for simultaneous microstructural and molecular imaging in vivo. *Nat. Med.* **17**, 1680–1684 (2011).
146. Park, J. et al. A dual-modality optical coherence tomography and fluorescence lifetime imaging microscopy system for simultaneous morphological and biochemical tissue characterization. *Biomed. Opt. Express* **1**, 186–200 (2010).
147. Liu, L. et al. Imaging the subcellular structure of human coronary atherosclerosis using micro-optical coherence tomography. *Nat. Med.* **17**, 1010–1014 (2011).
148. de Boer, J. F., Hitzenberger, C. K. & Yasuno, Y. Polarization sensitive optical coherence tomography-a review [Invited]. *Biomed. Opt. Express* **8**, 1838–1873 (2017).

149. Tearney, G. J. et al. In vivo endoscopic optical biopsy with optical coherence tomography. *Science* **276**, 2037–2039 (1997).
150. Yun, S., Tearney, G., de Boer, J., Iftimia, N. & Bouma, B. High-speed optical frequency-domain imaging. *Opt. Express* **11**, 2953–2963 (2003).
151. Kim, J. S. et al. Neointimal patterns obtained by optical coherence tomography correlate with specific histological components and neointimal proliferation in a swine model of restenosis. *Eur. Heart J. Cardiovasc. Imaging* **15**, 292–298 (2014).
152. Gonzalo, N. et al. Optical coherence tomography patterns of stent restenosis. *Am. Heart J.* **158**, 284–293 (2009).

Acknowledgements
I.-K.J.'s research is supported by Mrs Gillian Gray through the Allan Gray Fellowship Fund in Cardiology.

Author contributions
M.A. and I.-K.J. discussed the content of the article and wrote the manuscript. All the authors reviewed and/or edited the manuscript before submission.

Competing interests
H.L.D. is a consultant to Baim Clinical Research Institute, Boston Scientific, Cardiovascular Research Foundation and Medtronic, and has research grants from Boston Scientific and Medtronic. S.U. received educational grants from Abbott Vascular Japan. J.-S.K. received proctoring fees from Abbott Vascular. C.D.M. received research grants (to the institution) from AMGEN, Behring, Boston Scientific, Chiesi, Daiichi-Sankyo, Edwards, Medtronic, and Shockwave Volcano-Philips and speaker fees from Abbott and Shockwave. T.W.J. received consultancy and speaker fees from Abbott Vascular & Terumo. G.G. received consultant fees from Abbott Vascular and Infraredx and research grants from Abbott Vascular, Amgen and Infraredx. M.J. received personal fees from Abbott, AstraZeneca, Biotronik, Boston Scientific, Edwards, OrbusNeich, Recor, and Shockwave and grants from Amgen, Boston Scientific, Cardiac Dimensions, Edwards and Infraredx. N.R.H. received speaker fees from Terumo, research grants and speaker fees from Abbott and Reva Medical, and research grants from B. Braun, Biosensors, Boston Scientific and Medis Medical Imaging. W.W. received institutional research grants and honoraria from MicroPort (steering Committee TARGET AC trial); is co-founder of Argonauts, an innovation facilitator; and is medical adviser to Rede Optimus Research and Corrib Core Laboratory, NUI Galway. T.Adriaenssens received educational grants from Abbott Vascular. H.N. received speaker honoraria and research grants from Abbott Vascular. N.A. received proctoring and consulting fees from Abbott Vascular and Boston Scientific, consulting fees from Shockwave Medical, and institutional research grants from Abbott Vascular. G.S. received consulting fees from Abbott Medical, Boston Scientific, Medtronic, Shockwave and Terumo. E.G. is a consultant for Abbott Vascular and Terumo. N.G. received speaker and consultant fees from Abbott and speaker fees from Boston Scientific. G.J.T. receives sponsored research funding from AstraZeneca, Canon, CN USA Biotech Holdings, and VivoLight and catheter materials from Terumo. G.J.T. has a financial/fiduciary interest in SpectraWave, a company developing an OCT–NIRS intracoronary imaging system and catheter; this financial/fiduciary interest was reviewed and is managed by the Massachusetts General Hospital and Mass General Brigham HealthCare in accordance with their conflict-of-interest policies. G.J.T. (Canon, Spectrawave and Terumo) has the right to receive royalties from licensing arrangements. B.B. has OCT patents assigned to Massachusetts General Hospital and licensed to Terumo. A.D.A. received research grants from Amgen and Philips Healthcare. G.S.M. received honoraria from Abiomed, Boston Scientific, Medtronic and Philips/Volcano, and has equity in SpectraWave. G.W.S. received speaker honoraria from Cook, Infraredx and Terumo; is a consultant to Ablative Solutions, Abiomed, Ancora, Cardiomech, CorFlow, Elucid Bio, Gore, HeartFlow, MAIA Pharmaceuticals, Miracor, Neovasc, Occlutech, Reva, Robocath, Shockwave, TherOx, Valfix, Vascular Dynamics, Vectorious and V-Wave; and has equity/options from Ancora, Applied Therapeutics, Aria, Biostar family of funds, Cagent, Cardiac Success, MedFocus family of funds, Orchestra Biomed, SpectraWave and Valfix. L.R. received grants to the institution from Abbott, Biotronik, Boston Scientific, Heartflow, Sanofi, and Regeneron and speaker/consultation fees from Abbott, Amgen, AstraZeneca, Canon, Occlutec, Sanofi and Vifor. T.S. received research grants from Abbott Medical Japan. B.P.Y. received research grants and speaker honorarium from Abbott Vascular. L.K.M. received departmental grants from Abbott. H.R. received donations for research from Abbott Vascular, BioTelemetry and Siemens. P.L. is an unpaid consultant to, or involved in clinical trials for Amgen, AstraZeneca, Baim Institute, Beren Therapeutics, Esperion Therapeutics, Genentech, Kancera, Kowa Pharmaceuticals, Medimmune, Merck, Norvo Nordisk, Novartis, Pfizer, Sanofi-Regeneron. P.L. is a member of scientific advisory board for Amgen, Caristo, Cartesian, Corvidia Therapeutics, CSL Behring, DalCor Pharmaceuticals, Dewpoint, Kowa Pharmaceuticals, Medimmune, Novartis, Olatec Therapeutics, PlaqueTec and XBiotech. P.L.'s laboratory has received research funding in the past 2 years from Novartis. P.L. is on the Board of Directors of XBiotech. P.L. has a financial interest in Xbiotech, a company developing therapeutic human antibodies. P.L.'s interests were reviewed and are managed by Brigham and Women's Hospital and Partners HealthCare in accordance with their conflict-of-interest policies. G.W. is a member of the medical advisory board for Filterlex, Intratech, Microbot and Trisol, and received equity from Filterlex, Intratech and Microbot and consulting fees from Cuspa, Filterlex, Intratech, Magenta and Microbot. T.G. received speaker's honoraria and research support from Abbot Vascular. K.T. received research grants from Medtronic, and is proctor for Abbott and Medtronic. T.Y. received an endowment from Abbott Vascular Japan, Boston Scientific Japan, Japan Lifeline, Takeyama KK and WIN International. Y.M. received an honorarium and consulting fee from Abbott. R.Vergallo received speaker fees from Abbott. E.A. received grants from the Ministry of Health to the National IRCCS Cardiology Network (RCR-2019-23669116-001 and RCR-2020-23670065) and from FRRB grant CP_14/2018, INTESTRAT-CAD, Lombardia Region, Italy. H.M.G.-G. received institutional grant support from Abbott, Biotronik, Boston Scientific, CorFlow, Medtronic, Neovasc, Philips and Shockwave. Z.A. received institutional grants from Abbott Vascular and Cardiovascular Systems to Columbia University and Cardiovascular Research Foundation; honoraria from Amgen, AstraZeneca and Boston Scientific; and equity from Shockwave. A.V.F. and R.Virmani received institutional research support from NIH (HL141425), Leducq Foundation Grant; 480 Biomedical, 4C Medical, 4Tech, Abbott, Accumedical, Amgen, Biosensors, Boston Scientific, Cardiac Implants, Celonova, Claret Medical, Concept Medical, Cook, CSI, DuNing, Edwards Lifesciences, Emboline, Endotronix, Envision Scientific, Lutonix/Bard, Gateway, Lifetech, Limflo, MedAlliance, Medtronic, Mercator, Merill, Microport Medical, Microvention, MitraAlign, Mitra Assist, NAMSA, Nanova, Neovasc, NIPRO, Novogate, Occulotech, OrbusNeich Medical, Phenox, Profusa, Protembis, Qool, Recor, Senseonics, Shockwave, Sinomed, Spectranetics, Surmodics, Symic, Vesper, W.L. Gore and Xeltis. A.V.F. received honoraria from Abbott Vascular, Biosensors, Boston Scientific, Celonova, Cook Medical, CSI, Lutonix Bard, Sinomed and Terumo; and is a consultant to Amgen, Abbott Vascular, Boston Scientific, Celonova, Cook Medical, Lutonix Bard and Sinomed. R.Virmani received honoraria from Abbott Vascular, Biosensors, Boston Scientific, Celonova, Cook Medical, Cordis, CSI, Lutonix Bard, Medtronic, OrbusNeich Medical, CeloNova, SINO Medical Technology, ReCore, Spectranetics, Terumo, and W. L. Gore and is a consultant for Abbott Vascular, Boston Scientific, Celonova, Cook Medical, Cordis, CSI, Edwards Lifesciences, Lutonix Bard, Medtronic, OrbusNeich Medical, ReCore, Sinomededical Technology, Spectranetics, Surmodics, Terumo, W. L. Gore and Xeltis. T.K. received personal fees from Abbott Japan. K.H. received remuneration for lectures from Terumo, Abbott Vascular and Boston Scientific Japan. T.Akasaka received research grants from Abbott Vascular Japan, Nipro, and Terumo and is a medical adviser for Terumo. A.L. received consultant fees from Volcano and Philips. E.R. is a member of the medical advisory board for Zed Medical and a clinical adviser for Kaminari Medical. B.Y. received research grants from the National Key R&D Program of China (2016YFC1301103) and the National Natural Science Foundation of China (81827806). F.C. received personal fees from Amgen, AstraZeneca, BMS and Servier, and other fees from GlyCardial Diagnostics. J.F. has financial interests in Optovue, receives royalties from intellectual property owned by MIT and licensed to Optovue and receives research support from the NIH and Topcon. I.-K.J. received educational grants from Abbott Vascular and consulting fees from Mitobridge and Svelte. The other authors declare no competing interests.

Peer review information
Nature Reviews Cardiology thanks Antonio Colombo, Patrick Serruys and the other, anonymous, reviewer(s) for their contribution to the peer review of this work.

Supplementary information
The online version contains supplementary material available at https://doi.org/10.1038/s41569-022-00687-9.

Makoto Araki[1], Seung-Jung Park[2], Harold L. Dauerman[3], Shiro Uemura[4], Jung-Sun Kim[5], Carlo Di Mario[6], Thomas W. Johnson[7], Giulio Guagliumi[8], Adnan Kastrati[9], Michael Joner[10], Niels Ramsing Holm[11], Fernando Alfonso[12], William Wijns[13], Tom Adriaenssens[14], Holger Nef[15], Gilles Rioufol[16], Nicolas Amabile[17], Geraud Souteyrand[18], Nicolas Meneveau[19], Edouard Gerbaud[20], Maksymilian P. Opolski[21], Nieves Gonzalo[22], Guillermo J. Tearney[1], Brett Bouma[1], Aaron D. Aguirre[1], Gary S. Mintz[23], Gregg W. Stone[24], Christos V. Bourantas[25], Lorenz Räber[26], Sebastiano Gili[27], Kyoichi Mizuno[28], Shigeki Kimura[29], Toshiro Shinke[30], Myeong-Ki Hong[5], Yangsoo Jang[5], Jin Man Cho[31], Bryan P. Yan[32], Italo Porto[33], Giampaolo Niccoli[34], Rocco A. Montone[35], Vikas Thondapu[1], Michail I. Papafaklis[36], Lampros K. Michalis[36], Harmony Reynolds[37], Jacqueline Saw[38], Peter Libby[39], Giora Weisz[40], Mario Iannaccone[41], Tommaso Gori[42], Konstantinos Toutouzas[43], Taishi Yonetsu[44], Yoshiyasu Minami[45], Masamichi Takano[46], O. Christopher Raffel[47], Osamu Kurihara[46], Tsunenari Soeda[48], Tomoyo Sugiyama[49], Hyung Oh Kim[31], Tetsumin Lee[50], Takumi Higuma[51], Akihiro Nakajima[1], Erika Yamamoto[52], Krzysztof L. Bryniarski[53], Luca Di Vito[54], Rocco Vergallo[55], Francesco Fracassi[55], Michele Russo[55], Lena M. Seegers[1], Iris McNulty[1], Sangjoon Park[56], Marc Feldman[57], Javier Escaned[58], Francesco Prati[59], Eloisa Arbustini[60], Fausto J. Pinto[61], Ron Waksman[62], Hector M. Garcia-Garcia[62], Akiko Maehara[23], Ziad Ali[23], Aloke V. Finn[63], Renu Virmani[63], Annapoorna S. Kini[64], Joost Daemen[65], Teruyoshi Kume[4], Kiyoshi Hibi[66], Atsushi Tanaka[67], Takashi Akasaka[67], Takashi Kubo[67], Satoshi Yasuda[68], Kevin Croce[39], Juan F. Granada[23], Amir Lerman[69], Abhiram Prasad[69], Evelyn Regar[70], Yoshihiko Saito[71], Mullasari Ajit Sankardas[72], Vijayakumar Subban[72], Neil J. Weissman[73], Yundai Chen[74], Bo Yu[75], Stephen J. Nicholls[76], Peter Barlis[77], Nick E. J. West[78], Armin Arbab-Zadeh[79], Jong Chul Ye[56], Jouke Dijkstra[80], Hang Lee[1], Jagat Narula[24], Filippo Crea[55], Sunao Nakamura[81], Tsunekazu Kakuta[49], James Fujimoto[82], Valentin Fuster[24] and Ik-Kyung Jang[1,31] ✉

[1]Massachusetts General Hospital, Boston, MA, USA. [2]Asan Medical Center, Seoul, South Korea. [3]University of Vermont, Burlington, VT, USA. [4]Kawasaki Medical School, Okayama, Japan. [5]Yonsei University College of Medicine, Seoul, South Korea. [6]Careggi University Hospital, Florence, Italy. [7]University Hospitals Bristol and Weston NHS Foundation Trust, Bristol, UK. [8]Ospedale Papa Giovanni XXIII, Bergamo, Italy. [9]Technische Universität München and Munich Heart Alliance, Munich, Germany. [10]German Heart Center, Munich, Germany. [11]Aarhus University Hospital, Skejby, Denmark. [12]Hospital Universitario La Princesa, Madrid, Spain. [13]National University of Ireland Galway and Saolta University Healthcare Group, Galway, Ireland. [14]University Hospitals Leuven, Leuven, Belgium. [15]University of Giessen, Giessen, Germany. [16]Hospices Civils de Lyon and Claude Bernard University, Lyon, France. [17]Institut Mutualiste Montsouris, Paris, France. [18]University Hospital of Clermont Ferrand, Clermont-Ferrand, France. [19]University Hospital Jean Minjoz, Besançon, France. [20]University Hospital of Bordeaux, Pessac, France. [21]National Institute of Cardiology, Warsaw, Poland. [22]Hospital Clinico San Carlos, IdISSC, Universidad Complutense, Madrid, Spain. [23]Cardiovascular Research Foundation, New York, NY, USA. [24]Icahn School of

Medicine at Mount Sinai, New York, NY, USA. [25]Barts Health NHS Trust, University College London and Queen Mary University London, London, UK. [26]Inselspital, Bern University Hospital, University of Bern, Bern, Switzerland. [27]Centro Cardiologico Monzino, IRCCS, Milan, Italy. [28]Mitsukoshi Health and Welfare Foundation, Tokyo, Japan. [29]Yokohama Minami Kyosai Hospital, Kanagawa, Japan. [30]Showa University Hospital, Tokyo, Japan. [31]Kyung Hee University, Seoul, South Korea. [32]Chinese University of Hong Kong, Hong Kong, Hong Kong. [33]University of Genoa, Genoa, Italy, San Martino Hospital, IRCCS for Oncology and Neurosciences, Genoa, Italy. [34]University of Parma, Parma University Hospital, Parma, Italy. [35]Fondazione Policlinico Universitario A. Gemelli IRCCS, Rome, Italy. [36]University Hospital of Ioannina, Ioannina, Greece. [37]New York University Grossman School of Medicine, New York, NY, USA. [38]Vancouver General Hospital, University of British Columbia, Vancouver, British Columbia, Canada. [39]Brigham and Women's Hospital, Boston, MA, USA. [40]New York Presbyterian Hospital, Columbia University Medical Center and Cardiovascular Research Foundation, New York, NY, USA. [41]Ospedale San Giovanni Bosco, Turin, Italy. [42]Universitäts medizin Mainz and DZHK Rhein-Main, Mainz, Germany. [43]National and Kapodistrian University of Athens, Athens, Greece. [44]Tokyo Medical and Dental University, Tokyo, Japan. [45]Kitasato University School of Medicine, Kanagawa, Japan. [46]Nippon Medical School Chiba Hokusoh Hospital, Chiba, Japan. [47]The Prince Charles Hospital, Chermside, Queensland, Australia. [48]Nara Medical University, Nara, Japan. [49]Tsuchiura Kyodo General Hospital, Ibaraki, Japan. [50]Japanese Red Cross Musashino Hospital, Tokyo, Japan. [51]Kawasaki Municipal Tama Hospital, St. Marianna University School of Medicine, Kanagawa, Japan. [52]Kyoto University Graduate School of Medicine, Kyoto, Japan. [53]Jagiellonian University Medical College, Institute of Cardiology, Department of Interventional Cardiology, John Paul II Hospital, Krakow, Poland. [54]Mazzoni Hospital, Ascoli Piceno, Italy. [55]Catholic University of the Sacred Heart, Rome, Italy. [56]Korea Advanced Institute of Science and Technology, Daejeon, South Korea. [57]University of Texas Health, San Antonio, TX, USA. [58]Hospital Clínico San Carlos, Madrid, Spain. [59]UniCamillus – Saint Camillus International University of Health Sciences, Rome, Italy. [60]IRCCS Foundation University Hospital Policlinico San Matteo, Pavia, Italy. [61]Santa Maria University Hospital, CHULN Center of Cardiology of the University of Lisbon, Lisbon School of Medicine, Lisbon Academic Medical Center, Lisbon, Portugal. [62]MedStar Washington Hospital Center, Washington, DC, USA. [63]CV Path Institute, Gaithersburg, MD, USA. [64]Mount Sinai Hospital, New York, NY, USA. [65]Erasmus University Medical Centre, Rotterdam, Netherlands. [66]Yokohama City University Medical Center, Kanagawa, Japan. [67]Wakayama Medical University, Wakayama, Japan. [68]Tohoku University Graduate School of Medicine, Sendai, Japan. [69]Mayo Clinic, Rochester, MN, USA. [70]University Hospital Zürich, Zürich, Switzerland. [71]Gifu University Graduate School of Medicine, Gifu, Japan. [72]Madras Medical Mission, Chennai, India. [73]MedStar Health Research Institute, Washington, DC, USA. [74]Sixth Medical Center, Chinese PLA General Hospital, Beijing, China. [75]The Second Affiliated Hospital of Harbin Medical University, Harbin, China. [76]Monash University, Melbourne, Victoria, Australia. [77]University of Melbourne, Melbourne, Victoria, Australia. [78]Royal Papworth Hospital, Cambridge, UK. [79]Johns Hopkins University, Baltimore, MD, USA. [80]Leiden University Medical Centre, Leiden, Netherlands. [81]New Tokyo Hospital, Chiba, Japan. [82]Massachusetts Institute of Technology, Cambridge, MA, USA. ✉e-mail:*ijang@mgh.harvard.edu*